Effect of bed roughness on the hydrodynamic properties of dam-break waves

M.J.P. Buitelaar

Master Thesis
June 2022

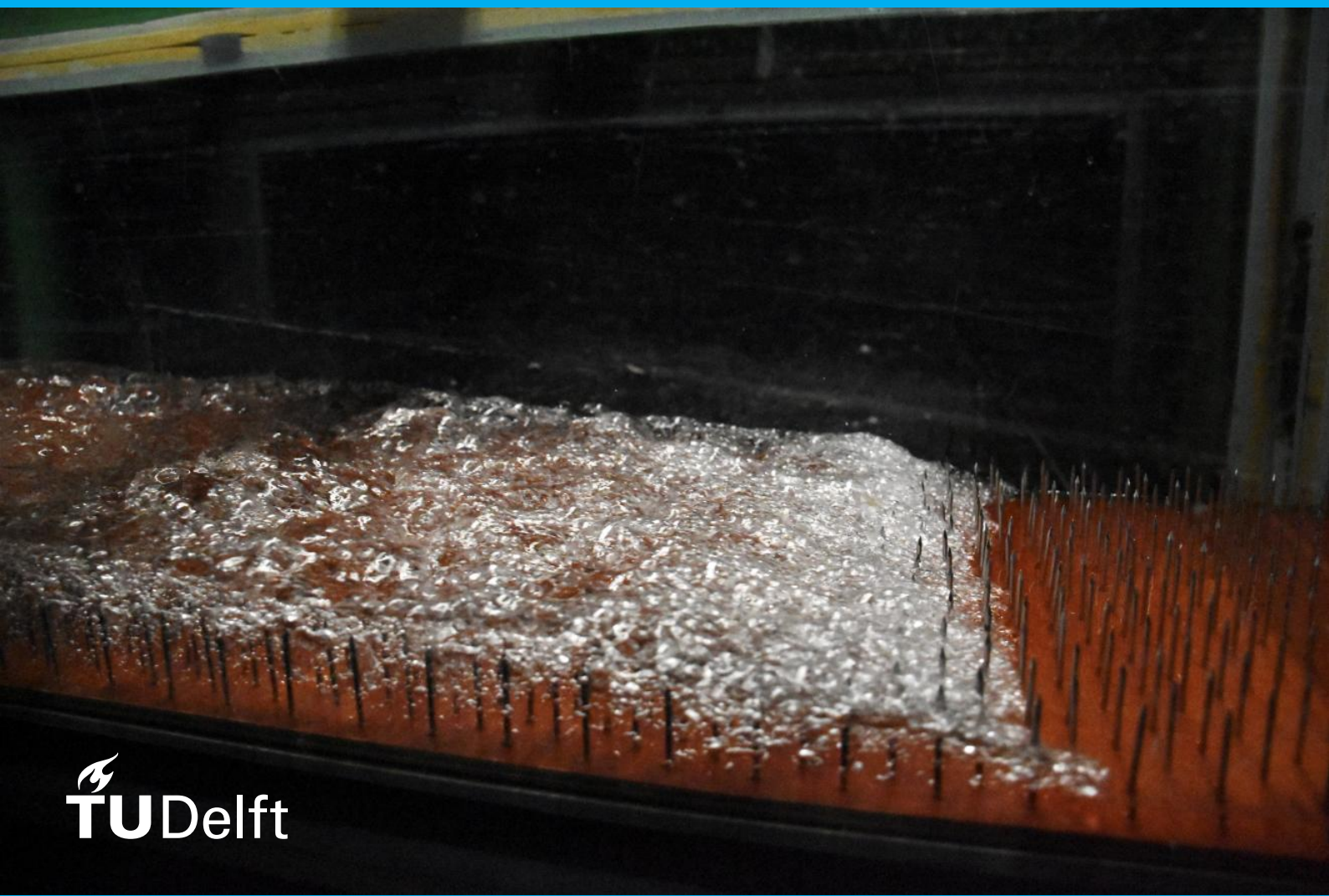

TU Delft

Effect of bed roughness on the hydrodynamic properties of dam-break waves

by

Maarten Jean-Pierre Buitelaar

in partial fulfilment of the degree of Master of Science
at the Delft University of Technology,
to be defended publicly on Tuesday June 14, 2022 at 10:00 AM.

This thesis is confidential and cannot be made public until June 14, 2023.

Student number:	4565355	
Project duration:	September 1, 2021 – June 14, 2022	
Thesis committee:	Dr. ir. Davide Wüthrich,	TU Delft, chair and daily supervisor
	Dr. ir. Bas Hofland,	TU Delft, supervisor
	Dr. Laura Stancanelli,	TU Delft, supervisor
	Dr. ing. Mark Voorendt,	TU Delft, supervisor

An electronic version of this thesis is available at `http://repository.tudelft.nl/`
The data obtained during this project can be found at `https://www.doi.org/10.4121/20017565`

Preface

This study represents the conclusion of my Master Civil Engineering, track Hydraulic Engineering, at Delft University of Technology. Over the past nine months, I have enjoyed working on this project, resulting in a master thesis report of which I am proud. However, I could never have done this entirely on my own, so I would like to thank the following people:

First of all, I would like to thank my committee: Bas Hofland, Laura Stancanelli, Mark Voorendt and Davide Wüthrich. Thank you for your time to give me guidance and feedback during the whole project. I really enjoyed working with you all. Special thanks to my daily supervisor Davide: thank you for your time and enthusiasm to guide me throughout the process.

I would like to thank the staff of the Hydraulic Engineering Laboratory of the TU Delft for their help with the test set-up and Ecole Polytechnique Fédérale de Lausanne for borrowing the Acoustic Distance Meters. Moreover, I want to thank the Hydraulic Engineering Laboratory of the TU Delft for funding the experimental part of the project.

Finally, I would like to thank my family and friends who always supported me. Without your support, I would never have come this far.

Maarten Buitelaar
Delft, June 2022

Abstract

A dam-break wave can result in considerable damages and casualties. Events that can lead to such waves include dike and dam breaches, storm surges and impulse waves. Dutch history is familiar with a number of coastal dike breaches during the Watersnoodramp but also river dike breaches have occurred, resulting in dam-break waves reaching far inland. Beyond the Netherlands, propagating walls of water could occur when dams of water reservoirs collapse, like the South Fork Dam in the USA and the Möhne Dam in Germany or tsunamis propagating inland. These examples show that more specific knowledge of the hydrodynamic behaviour of dam-break waves is necessary in the battle against water.

The impact of a dam-break wave can be reduced through a better understanding of the link between bed roughness and wave hydrodynamic properties. However, this link is currently poorly understood. The objective of the present study is therefore to study experimentally the effect of bed roughness on the hydrodynamic properties of dam-break waves, on both dry and wet beds The approach was to generate dam-break waves through a lift-gate and a reservoir with a depth d_0 = 0.4 m and to measure the water levels over time in the downstream channel. With gravel and nails, 7 different bed roughness configurations were made with a range of k_s = 0.6 to 48 mm in addition to smooth bed reference test. Dry bed tests were performed at least 5 times per bed roughness, 5 wet bed tests with an initially still water level (h_0) in a range of h_0/d_0 = 0 to 0.125 were performed at least 10 times per bed roughness. The analysis focused on wavefront celerity, inundation depths and roller length which are used to characterise the hydrodynamic properties of the wave.

Visual observations showed substantial differences in wavefront behaviour between dry bed surges and wet bed bores as well as between smooth and rough bed. Validation of the generated waves was done by successfully comparing the reconstructed water levels over the flume length with a new approach combining experimental data with theory and previous studies. The measured water depths over time showed different behaviours indicating that the four parameters are affected by dry or wet and smooth or rough beds.

Results showed that an increase in bed roughness resulted in a decrease in wavefront celerity for surges and that the initially still water level can work as a lubricant for bores. The initial still water level is dominant over the bed roughness when $h_0 > 0.5k_s$.

The maximum water level increased with increasing bed roughness for surges, while bores showed an opposite behaviour. Increasing the initially still water level reduced the relative maximum water level for rough bed configurations.

In the present study, only some test configurations revealed the presence of a plateau height. If there was one, an increase in bed roughness showed a decrease in plateau height for bores with h_0/d_0 = 0.125. Three sections in the h_0/d_0 range with different plateau height behaviours were noticed.

The roller lengths were determined with the wavefront celerity and the plateau height, if one was present. No trivial relations were found for the influence of bed roughness or initial still water level on the roller length of the bores.

Overall, this project revealed some interesting behaviours that need to be further investigated in the future. It is recommended to conduct a full quantitative analysis once precise values of the bed roughness configurations are determined. The estimation of the present bed roughness coefficients should be done through a deeper analysis of the boundary layer during steady flow tests. Nevertheless, these results present some preliminary, yet interesting, findings that will contribute to a better understanding of the behaviour of dam-break waves over rough bed.

List of Symbols

Symbol	Definition	Unit
c	wavefront celerity	m/s
c_{dam}	wavefront celerity at dam location	m/s
D_H	hydraulic diameter	m
d_p	plate thickness	m
d_0	reservoir depth	m
F	Froude number: $F = V/(gL)^{1/2}$	-
F_B	bore Froude number: $F_B = c/\sqrt{gh_0}$	-
f	Darcy-Weisbach friction factor	-
g	gravitational acceleration	m/s^2
h	water depth	m
h_r	roughness height	m
h_{max}	maximum water depth	m
h_2	plateau height of the wave	m
h_0	initial still water level	m
k_s	roughness height	m
L_r	roller length	m
L_x	development length	m
M	momentum flux per unit width	m^3/s^2
p	pressure	kg/ms^2
R	Reynolds number: $R = c \cdot D_H/h_0$	-
t	time after opening gate	s
t_0	wave arrival time	s
s	horizontal distance from the wave tip, positive upstream direction	m
U	wave celerity	m/s
V	inertial force	$kg \cdot m/s^2$
x	location in the flume downstream of the gate, positive downstream direction	m
x_s	wavefront location downstream of the gate	m
α	celerity coefficient	-
ν	kinematic viscosity	m^2/s
ν_t	nominal eddy-viscosity	m^s/s
ρ	water density	kg/m^3
σ	surface tension between air and water	kg/s^2

Contents

1

Introduction

1.1. Background

Propagating water level differences come in all shapes and sizes. Small differences in water level can be experienced as enjoyable waves (Figure 1.1), but larger differences could also cause considerable damages and sometimes casualties.

Figure 1.1: Tidal bore coming into the estuary of the River Kent in England (Arnold Price, CC BY-SA 2.0)

Dike or dam breaches are examples of phenomena that can lead to these types of waves. Dutch history is familiar with a number of dike breaches, including in 1953, during the Watersnoodramp, when several sea dikes failed. Well-known breaches occurred in the Alblasserwaard near Papendrecht, near Den Bommel (Figure 1.2) (Rijkswaterstaat, 2021) and near Stavenisse where 1800 metre length of dike was swept away in one go. During the Watersnoodramp 1,836 people lost their lives, 100,000 were made homeless and 2 billion m^2 of land were flooded (Watersnoodmuseum, 2018). An example of a breach in a river dike has been seen in the Maasdijk near Overasselt (Limburg) in 1926. This breach damaged 3,000 houses resulting in a total damage of 10 million guilders (Dute, 2008). A more recent example is the dike failure near Meerssen (Limburg) in the summer of 2021 (Meerssen, 2021). These examples show that potential dike breaches have been a relevant topic over the years and more specific knowledge of the hydrodynamic behaviour of dam-break waves can be very useful in the battle against water.

Figure 1.2: Dike breach Watersnoodramp Den Bommel, the Netherlands (Rijkswaterstaat, 2021)

Beyond the Netherlands, water level differences could occur when dams of water reservoirs collapse. The sudden total failure of such dams leads to a large amount of water propagating downstream with dreadful consequences for people and for the natural and built environment. Two examples of these dam failures are the South Fork (Johnstown) Dam in the USA (Figure 1.3a) and the Möhne Dam in Germany (Figure 1.3b) with more than 2,000 and 1,300 deaths respectively (Chanson, 2004a). In both dam failures, there was no overtopping but a large section of the dam failed at once, causing a wall of water flowing downstream.

(a) Dam-break South Fork Dam, USA (WaterArchives.org, CC BY-SA 2.0)

(b) Dam-break Möhne Dam, Germany (Bundesarchiv, CC-BY-SA 3.0)

Figure 1.3: Two examples of dam breaches with a sudden failure causing a wall of water

Furthermore, tsunamis are examples of moving water level differences. They mainly cause damage on land, as was the case with the tsunamis on Sumatra (Indonesia) in 2004 and Honshu (Japan) in 2011 (Figure 1.4). Over 130,000 and 20,000 people were killed respectively and caused enormous damages (Humanity House, 2017; Rafferty and Pletcher, 2011). Certain aspects of these long-period waves propagating inland resemble dam-break flow and numerical models for tsunamis are often validated against basic dam-break solutions (Chanson, 2006b). Also experimentally, dam-break waves are more and more often used to reproduce tsunami waves.

Figure 1.4: Tsunami near Honshu Japan 2011 (Rafferty, 2011)

Dam-break waves are the type of waves studied in this master thesis and will be reproduced during experimental tests.

1.2. Literature Review

Because of their importance, dam-break waves have been widely studied in the last century. A literature review is therefore given, covering the theory of dam-break waves, previous research on dam-break wave effects and the relevance of further research.

A general definition of a dam-break wave is an unsteady, non-uniform, violent flow that occurs after a certain volume of water is released (Nielsen, 2018). The reservoir upstream of the dam is an impounded volume that is released when a gate is opened or a dam fails completely. This causes a sudden difference in water head that creates the dam-break wave. A dam-break wave differs from steady flows because the variables, such as velocity and water depth, change with space and time (Aleixo et al., 2019).

1.2.1. Theory of Dam-Break Waves

Ritter (1892) presented theoretical solutions of the dam-break wave using a 1D approximation of the Navier-Stokes equations (Chanson, 2006a; Lauber and Hager, 1998a; Ritter, 1892) assuming an initially dry, smooth bed, for an ideal fluid and semi-infinite reservoir in a wide rectangular channel (Ritter, 1892). This generated a closed set of equations that describe the flow depth and flow velocity as a function of space and time (Figure 1.5). Ritter (1892) presented a formula for the wavefront celerity (c)

$$c = 2\sqrt{gd_0} \tag{1.1}$$

where g = gravity constant and d_0 = equivalent impoundment depth. The celerity at the gate location could be obtained via the following formula

$$c_{dam} = \frac{2}{3}\sqrt{gd_0} \tag{1.2}$$

The downstream water level (h), at a certain location downstream of the gate (x), at a certain moment in time (t) can be calculated with the following formula

$$h = d_0 \cdot \frac{1}{9}\left(2 - \frac{x}{t - \sqrt{gd_0}}\right)^2 \tag{1.3}$$

and leading to a constant water level of $h = 4/9d_0$ at the gate. All the assumptions lead to an unrealistic scenario that will never be encountered in real life. Moreover, the sharp wavefront is mathematically possible but physically impossible. For this, Whitham (1955) added bottom friction, applied to a real fluid, creating a modified dam-break wave theory, arguing that this leads to a more realistic wavefront, where bed friction

is predominant. The analytical solution was based upon the Pohlhausen technique and it treats the boundary layer integrally. Due to the friction component, it resulted in analytically non-solvable non-linear terms (Chanson, 2006a). The renewed formula for the wavefront celerity is given below and includes the Darcy-Weisbach friction factor (f).

$$c = \sqrt{gd_0} \cdot \left(2 - 3.452\sqrt{\frac{f}{8}t\sqrt{\frac{g}{d_0}}}\right) \tag{1.4}$$

The renewed formula for wave height in the downstream part of the flume is given below.

$$\frac{x - x_s}{d_0} = -\frac{f}{8} \cdot \frac{c^2}{g \cdot d_0} \cdot \left(\frac{g}{\delta c/\delta t}\right)^2 \cdot \left[\ln\left(1 + \frac{8}{f} \cdot \frac{h/d_0}{c^2/(g \cdot d_0)} \cdot \frac{\delta c/\delta t}{g}\right) + \frac{8}{f} \cdot \frac{h/d_0}{c^2/(g \cdot d_0)} \cdot \frac{\delta c/\delta t}{g}\right] \tag{1.5}$$

where x_s = wavefront location and $\delta c/\delta t$ = change of wavefront celerity over time.

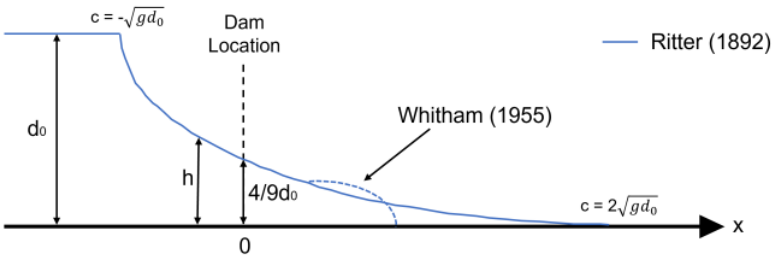

Figure 1.5: Overview of Ritter's (1892) and Whitham's (1955) theory for dry bed surges

Some empirical approximations for practical use were presented by Chanson (2004b). Dressler (1952) also introduced friction to Ritter's theory, starting with a simple wave. The non-linear shallow-water equations were used and resistance was added via the Chézy resistance formula. The wavefront became an envelope of characteristics due to resistance (Dressler, 1952; Leng and Chanson, 2014).

Stoker (1957) introduced also a theory with formulas for dam-break waves with an initially still water level downstream of the gate (Figure 1.6), treating the propagating wave as a shock. When an ideal fluid dam-break wave progresses into a resting tail-water with a horizontal bed, a quasi-steady bore develops after some distance (Stoker, 1957). The wave celerity is reduced and the wave tip is thickened by the opposing momentum of the tailwater (Stoker, 1957). Formulas for wavefront celerity for bores presented by Stoker are given below.

$$c = \sqrt{g\frac{h_0 + h_2}{2} \cdot \frac{h_2}{h_0}} \tag{1.6}$$

$$c = gh_0 \cdot \sqrt{\frac{1}{8} \cdot \left[\left(2\frac{h_2}{h_0} + 1\right)^2 - 1\right]} \tag{1.7}$$

where h_0 = initial still water level and h_2 = plateau height, the measured constant water level after the wavefront or calculated with an empirical formula (Eq. 1.10).

A particular application of the MacLaurin series for Stoker's (1957) theory for bore front celerities was recently developed by Nielsen et al. (2022) and resulted in the following formula

$$c_{ideal} = \sqrt{gd_0} \cdot \left(2 - 3.36\left(\frac{h_0}{d_0}\right)^{\frac{1}{4}} + 3.54\left(\frac{h_0}{d_0}\right)^{\frac{1}{2}} - 1.49\left(\frac{h_0}{d_0}\right)^{\frac{3}{4}} + 0.12\frac{h_0}{d_0} - ...\right) \tag{1.8}$$

There is no unique theory that is best applied to all types of dam-break waves, but the most suitable depends on its main application. Dressler's (1952) method treated the wave leading edge as an approximation, but is a very robust method that can so be used in several different cases. Using Whitham's (1955) method resulted

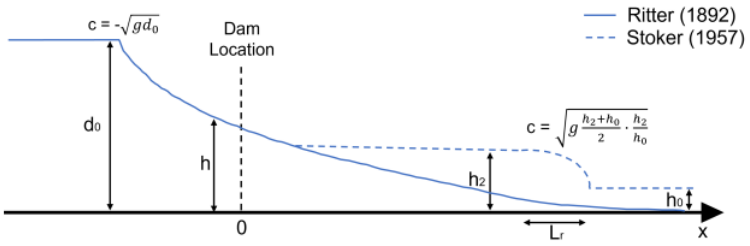

Figure 1.6: Overview of Stoker's (1957) wet bed bore theory

in an asymptotic solution. Chanson's (2004b) method provided explicit solutions, which are easy for practical use, especially in the engineering practice. All assumed a constant friction factor, which is debatable for real-life situations (Chanson, 2006a). Later, an additional analytical solution was presented including a non-constant friction factor for laminar and turbulent flow motions of dam-break waves by Chanson (2006a). This theory is only applicable to rectangular channels with quasi-instantaneous dam breaks from a limited semi-infinite reservoir (Chanson, 2006a). The downstream water level can be calculated with the following formula

$$h = d_0 \cdot \sqrt{\frac{f}{4} \cdot \left(\frac{U}{\sqrt{g d_0}}\right)^2 \cdot \left(\frac{x - x_s}{d_0}\right)} \tag{1.9}$$

The plateau height can be obtained with the empirical formula below

$$h_2 = d_0 \cdot 0.932 \left(\frac{h_0}{d_0}\right)^{0.371} \tag{1.10}$$

Moreover, a new formula for the wavefront celerity is presented with the empirical approximation of Montes (1998):

$$c = \sqrt{g \cdot h0} \cdot \frac{0.63545 + 0.3286 \left(\frac{h_0}{d_0}\right)^{0.65167}}{0.00251 + \left(\frac{h_0}{d_0}\right)^{0.65167}} \tag{1.11}$$

Furthermore, Chanson (2006b) showed that a dam-break wave could be used to describe tsunamis propagating on land. A clear overview of all the formulas that can be used for dry and wet bed, with and without resistance situations can be found in Henderson (1996) and Chanson (2004b). Using a wave generator in a laboratory resulted in too short waves to represent a tsunami wave (Madsen et al., 2008). Therefore, a dam-break wave can offer a more realistic representation of the physical process.

As described above, Stoker (1957) stated that the bore becomes quasi-steady after some distance. Nielsen et al. (2022) came up with a formula to calculate this development length (L_x)

$$L_x \approx 2.1 \cdot d_0^{6/5} k_s^{-1/5} \tag{1.12}$$

where k_s = average bed roughness height.

The coefficient in Equation 1.1 to calculate the wavefront celerity for Ritter's (1892) theory can be changed to look for a better fit with tests including bed roughness or initially still water levels. This results in Equation 1.13.

$$c = \alpha \cdot \sqrt{g d_0} \tag{1.13}$$

Nielsen et al. (2022) recently presented a model to calculate the wavefront celerity, taking into account bed roughness (Equation 1.14) or both initially still water levels and small bed roughnesses ($k_s/d_0 < 0.01$) (Equation 1.15). The effect of bed roughness and viscosity on dry beds were similar to effects of initial still water levels when the friction lengths (k_s/d_0 and $\nu/\sqrt{g d_0^3}$) were small.

$$c_{ideal} = \sqrt{gd_0} \cdot \left(2 - 3.4\left(13\frac{k_s}{d_0}\right)^{\frac{1}{4}} + 3.5\left(13\frac{k_s}{d_0}\right)^{\frac{1}{2}} - 1.5\left(13\frac{k_s}{d_0}\right)^{\frac{3}{4}} + 0.12\left(13\frac{k_s}{d_0}\right)\right) \tag{1.14}$$

$$\frac{c_{ideal}}{\sqrt{gd_0}} = F\left(\frac{h_0 + 13k_s + 1700\nu/\sqrt{gd_0}}{d_0}\right) \tag{1.15}$$

The time required for a dam-break wave to rise to the plateau height is the roller time. When this value is multiplied by the wavefront velocity, the roller length can be obtained. In previous studies, Chanson (2011); Wüthrich et al. (2018), analysed the roller lengths of experimental tests and presented their optimal fits for the rising water levels. The following formula was used in these studies:

$$\frac{h - h_0}{h_2 - h_0} = \left(\frac{x - x_s}{L_r}\right)^N \tag{1.16}$$

The best fitting exponents for Chanson (2011) N = 0.441 and for Wüthrich et al. (2018) N = 0.482.

A dam-break wave is influenced by many factors such as water height difference, viscosity, the slope of the channel (Lauber and Hager, 1998b) and the roughness of the bed in the channel (Wüthrich et al., 2019). It is important to consider the influence of a dry bed in the channel or a layer of water in the channel (wet bed) (Wüthrich et al., 2018, 2019), whose differences are discussed in Section 1.2.2. The effect of the bed roughness of the channel will be the focus of the research in this report and some literature is provided in Section 1.2.3.

1.2.2. Dry Bed Surges versus Wet Bed Bores

A distinction can be made between dry bed surges and wet bed bores depending on whether water is present in the downstream channel before the breach. This division can be made because even the presence of a thin still water layer in the downstream channel strongly influences the hydrodynamic behaviour of the dam-break wave. The wave then generated a fully turbulent bore front with substantial air-entrainment and entrapment (Wüthrich et al., 2018).
Since 1961, the difference between dam-break waves on dry (surge) and wet beds (bore) has been studied (Faure and Nahas, 1961). Hereafter is a brief overview of the main differences between surges and bores that emerged from previous research:

- Wet bed bores and dry bed surges have different wavefront behaviour (Wüthrich et al., 2015). While the dry bed solution is best described by Ritter (1892), the wet bed bore is better described by Stoker (1957). A division is made into four different phases of the wet bore: the turbulent front, a plateau (constant water height), a far back region (Ritter's theory applicable) and the upstream reservoir. The dry bed surge shows a sudden rise in water level and an immediately decreasing limb (Wüthrich et al., 2016, 2018). So, the difference between the dry bed surge and the wet bed bore is the presence of a **plateau** in the case of wet bed bores.

- The wet bed bore travels with a **lower wavefront celerity** than the dry bed surge for the same roughness values (Wüthrich et al., 2018).

- A wet bed bore has a **steeper wave front** compared to a dry bed surge (Wüthrich et al., 2015).

- The **influence of bed roughness** was shown to differ between dry bed surges and wet bed bores. For $h_0/d_0 > 0.037$ similar water level profiles over time at the same location were measured by Wüthrich et al. (2018). Below this limit, a transitional bore was observed with behaviour comparable to a dry bed surge. The wavefront celerity is thereby dependent on the height of the initial still water depth (Wüthrich et al., 2016). The influence of bed roughness is further evaluated in Section 1.2.3.

- A difference in the **breaking process** of the wave just after the gate is clearly visible (Wüthrich et al., 2016). For dry bed surges, no major aeration was observed, while this was the case for wet bed bores (Wüthrich et al., 2015). The bores showed recirculating rollers propagating over the initially still water level in the channel.

- A change in **Froude number** at the wave tip region was observed by Wüthrich et al. (2018). Dry bed surges are super-critical in the first phase of the flow subsequently reaching to the asymptotic value. Wet bed bores showed a more constant flow pattern for the whole wave. This difference between surges and bores becomes more important as the still water level in the channel increases. The bore Froude number was defined as $F_B = c/\sqrt{gh_0}$.

1.2.3. Effect of Bed Roughness

Roughness can be expressed in many different ways, such as Chézy (C), Manning-Strickler (n), Nikuradse coefficient (k_s) and Darcy-Weisbach friction factor (f). This study is focused on the Darcy-Weisbach friction factor, because this one is the most applied for bed roughness on dam-break waves and so values could be compared to literature (Chanson, 2004a).

Research into the influence of bed roughness on a dam-break wave, i.e. highly unsteady flow, has been conducted for some time. Schoklitsch (1917) performed already tests in 1917. In 1961, a physical experiment was carried out for the first time by Escande et al. (1961), where testing was done with a scaled model of a valley with different bed roughnesses. In these tests, it was shown that inclusion of a realistic roughness had a major impact on the wave celerity. This was also later confirmed in experiments by Wüthrich et al. (2019) and Esteban et al. (2020). An overview of previously performed dam-break waves is given in Table 1.1, including the dimensions of the flume, the instrumentation and the test program.

Previous tests used rubber mats and wooden panels (sometimes covered with gravel) to reproduce different roughness values often in a range of Darcy-Weisbach friction factors f= 0.02 (smooth) to f= 0.045 (rough) (Docherty and Chanson, 2010; Wüthrich et al., 2019). In these cases, several roughnesses were used and were then converted to the equivalent roughness height (k_s) (Esteban et al., 2020). Literature shows that increasing the bed roughness in a channel has the following effects on dam-break waves:

- A **higher flow depth** for dry bed surges. Which implies a higher inundation depth (up to 20%) downstream of the dam-break (Wüthrich et al., 2019).
- A **reduction of wavefront celerity** (Docherty and Chanson, 2012; Esteban et al., 2020; Wüthrich et al., 2019). Dressler (1952) and Whitham (1955) presented a theory that the bed friction reduces the wavefront celerity for dry bed surges. Research from Escande et al. (1961) stated that the wave celerity could be 20-30% lower if a very rough bed was placed in their channel under the same experimental conditions. This influences also the α-value (dimensionless celerity coefficient) used for calculating the wave celerity: $c = \alpha\sqrt{gd_0}$ (Eq. 1.13) (Wüthrich et al., 2018, 2019). At present, there is no relationship between α and the bed roughness available in literature.
- A **steeper wavefront** was observed in tests performed by Esteban et al. (2020). The water layer close to the bed is slowed down by the bed roughness. The bed friction has a thickening effect on the wavefront tip (Dressler, 1952).
- A **lower momentum flux** per unit width ($M = hU^2$) and **lower impact forces** (Wüthrich et al., 2019).
- **Shorter impact durations** and therefore **lower total impulses** (Wüthrich et al., 2019).
- A **higher required eddy viscosity** as ν_t scales with k_s (Nielsen, 2018).
- **More efficient dissipation of eddies** inside the flow and so result in a lower level of surface turbulence with fewer fluctuations. The dissipation is more efficient due to the larger turbulence intensities for rough beds (Wüthrich et al., 2016).
- **Longer and higher recirculation regions** in the recirculation 'bubble' immediately after the roller passage above the rough bed (Docherty and Chanson, 2012).

In addition to this list of effects associated with bed roughness, it should be noted that some research showed that the effect of roughness can become negligible for a sufficiently high initial still water level. Wüthrich et al. (2016, 2018) stated that similar velocities and height profiles were found for tests with the following criterion $h_0/d_0 > 0.037$. This outcome may hint that the importance of the change in roughness on wet bed bores is less influential compared to the initial still water level in the channel.

Article	d_0 (m)	Size LxWxH (m)	Slope	Gate system	h_0 (m)	Instrumentation	Number of repetitions	Roughness	Reservoir volume (m^3)
Aleixo et al. (2019)	0.325	6.0 x 0.25 x 0.5	-	vertical slide gate (slides downward)	0	PIV + PFC	7	smooth	0.4875
Esteban et al. (2020)	0.30-0.60	R: 14.0 × 0.41 × 0.6 D: 9.5 x 0.41 x 0.6	-	vertical slide gate	0-0.2	HS + WG + ECM	-	n = 0.02-0.06	18.9-37.8
Hooshyaripor et al. (2017)	0.35	R: 4.5 x 2.25 D: 9.3 x 0.51 x 0.7	-	vertical slide gate (pneumatic jack)	0	ADV	-	smooth	3.54
LaRocque et al. (2013)	0.25-0.35	R: 3.37 x 0.18 x 0.42 D: 3.94 x 0.18 x 0.42	0.93%	vertical slide gate (guillotine-type)	0	ADM + UVP	24	smooth	0.152-0.212
Lauber and Hager (1998a)	0.3	R: 3.5 x 0.5 x 1.2 D: 10.5 x 0.5 x 0.7	-	vertical slide gate	0	PIV + camera	-	PVC	0.525
Lauber and Hager (1998b)	0.3	R: 3.5 x 0.5 x 1.2 D: 10.5 x 0.5 x 0.7	50%	vertical slide gate	0	PIV + camera	-	PVC	0.525
Nielsen (2019)	0.43	width: 0.5	-		0	ADM	-	k_s = 65 mm	
Nielsen et al. (2022)	0.4	13 x 0.5 x 0.45	-	vertical slide gate	0-0.14	ADM	9	Smooth–k_s = 84 mm	0.6
Stolle et al. (2018)	0.20-0.40	30 x 1.5 x 0.80	-	vertical slide gate	0	WG + HS	14-30	f = 0.014	-
Stolle et al. (2019)	0.20-0.50	R: 21.55 × 1.5 × 0.80 D: 8.45 x 1.5 x 0.80 (0.20 m false floor)	-	swing gate	Thin water layer	WG + HS	1-3	f = 0.014	6.465-16.1625
Wüthrich et al. (2015)	0.3	R: 2.1 x 3.0x 1.0 D: 14 x 1.4	-	Pulleys and valves	0-0.05	ADM + HS + GoPro + UVP	-	smooth	7
Wüthrich et al. (2016)	0.7	R: 2.1 x 3.0x 1.0 D: 14 x 1.4	-	Pulleys and valves	0-0.05	ADM + PFC	-	f = 0.01-0.04 k_s =2.8	7
Wüthrich et al. (2018)	0.40-0.82	R: 2.1 x 3.0 x 1.0 D: 15.5 x 1.4	-	Pulleys and valves	0-0.1	ADM + UVP	-	k_s = 0.66 mm	7.08
Wüthrich et al. (2019)	0.4-0.82	R: 2.1 x 3.0 x 1.0 D: 15.5 x 1.4	-	Pulleys and valves	0	ADM + UVP	2-6	k_s = 0.66-2.8 mm	7
Xu et al. (2021)	0.4	D: 12.18 x 0.25	-	vertical slide gate	0-0.098	ADM + shear plate	-	k_s = 84 mm	-

Table 1.1: Literature overview characteristics dam-break waves tests. Abbreviations for size flume: L = length; W = width; H = height; R = reservoir; D = downstream flume. Abbreviations for instrumentation: ADM = Acoustic Distance Meter; UVP = Ultrasound Velocity Profiler; HS = High-speed Camera; WG = Wave Gauge; ECM = Electromagnetic Current Meter; PIV = Particle Image Velocimetry; PFC = Photron Fast Camera

A relationship between the water depths and the celerity was derived by Baldock (2018); Nielsen (2018, 2019):

$$h \sim \sqrt[4]{\frac{c^3 \nu_t s}{g^2}} \sim s^{1/4} \text{ with } c = \sqrt{g d_0} \tag{1.17}$$

where ν = eddy viscosity and s = horizontal distance from the wave tip, positive in upstream direction. The wavefront celerity is theoretically dependent on the roughness of the bed. Moreover, the nominal eddy-viscosity (ν_t) is also affected by roughness. However, the above formula was not tested against experimental data and no direct link was provided with the roughness, if not implicitly through the bore front celerity.

The number of tests should be reduced to prevent loss of time with unnecessary tests but the number of tests should also be sufficient to allow for reliable conclusions (Leng and Chanson, 2015). The number of tests that are presented in literature differs significantly in a range of 5 to 100 runs or tests per type of experiment (Figure1.7) (Aleixo et al., 2019; Esteban et al., 2020; Leng and Chanson, 2014; Reichstetter and Chanson, 2013; Wüthrich et al., 2020). The accuracy of the result increased as more tests are performed. The solid lines in Figure 1.7 indicate this phenomenon and present the number of tests performed in selected previous literature.

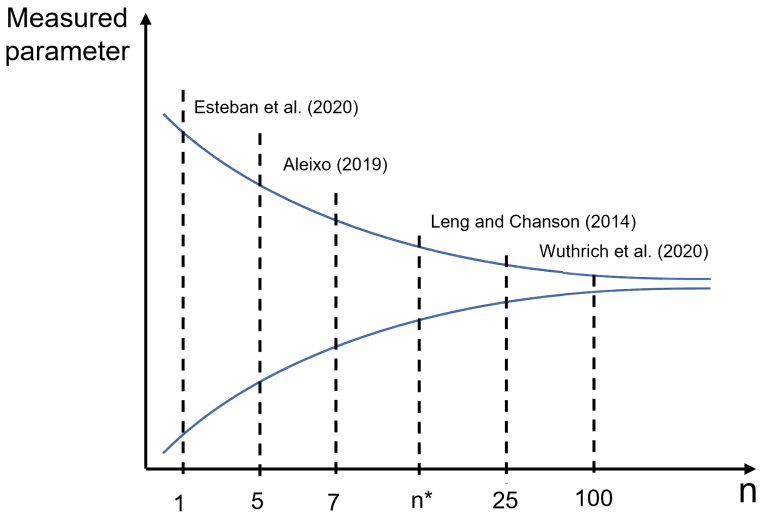

Figure 1.7: Number of tests used in previous studies. Solid lines indicate the increase of accuracy when the number of tests is increased

1.3. Problem Statement

Examples provided in the introduction pointed out the catastrophic nature of dam-break waves and the importance that wave propagation has on the development of its hydrodynamic properties. The impact of a dam-break wave or tsunami propagating on land can be reduced by a better understanding of the link between bed roughness and wave hydrodynamic properties. The inclusion of macro roughness in existing models is necessary to give a realistic picture of the phenomena being studied (Wüthrich et al., 2019). A potential link between bed roughness and hydrodynamic properties of dam-break waves is therefore missing. In addition, previous research has mostly produced qualitative results, pointing out the need for more quantitative ones. The literature review highlights four key parameters describing the hydrodynamic properties of a dam-break wave that are not yet well understood: c, h_{max}, h_2 and L_r.

1.4. Research Objective

The objective of this master thesis is to fill this research gap and answer the following main and sub-questions. Main research question: What is the effect of bed roughness on the hydrodynamic properties of dam-break waves, on both dry and wet beds?

- Sub-question 1: How can dam-break waves be reproduced and validated in a laboratory environment?
- Sub-question 2: How is wavefront celerity of a dam-break wave affected by bed roughness?
- Sub-question 3: How is the maximum water depth of a dam-break wave affected by bed roughness?
- Sub-question 4: What is the combined effect of an initially still water layer and bed roughness on the hydrodynamic properties of dam-break waves?

1.5. Report Outline

The research questions will be answered through experimental testing and data analysis. The complexity of the phenomena involved imposes the use of an experimental approach and not enough previous data is available to answer the previously mentioned research questions. Dam-break wave tests will be performed on dry, wet, smooth and rough beds.

In Chapter 1, the reader was given an introduction to the topic, a literature review, the significance of the study and the research problem. The generation of a dam-break wave and measurement techniques during the tests are described in Chapter 2. Chapter 3 presents the methodology of the experimental tests and describes the data processing procedure. The visual observations and validation of the dam-break wave facility are described in Chapter 4. Chapter 5 presents the obtained measurement results and the analysed data is displayed for the four parameters: c, h_{max}, h_2 and L_r. In Chapter 6 a discussion is given, followed by the conclusions and recommendations in Chapter 7.

2

Experimental Set-up

This Chapter describes the generation of dam-break waves, creating of bed roughness, the test protocol, the experimental program and scale effects, for maximum reliability of the laboratory experiments at prototype scale. Attention will be paid to the flume characteristics, gate opening mechanism and instrumentation.

2.1. Generation of Dam-Break Waves

The dam-break wave tests took place in the 1st tilting flume (West) at the Hydraulic Engineering Laboratory at the TU Delft (Figure 2.1). The flume has a length of 14.3 m, a width of 0.40 m and a height of 0.42 m. At the downstream end of the flume, water was drained to prevent reflection waves. The sidewalls of the flume are made of glass and the bottom was made of PVC. A gate opening mechanism was built into this flume, specifically for these tests, as shown in Figure 2.2. The flume was horizontal and the dam-break gate was installed at 6.8 m from the channel inlet, resulting in a reservoir volume of approximately 1.3 m^3.

Figure 2.1: Tilting flume in the Hydraulic Engineering Laboratory at the TU Delft

The gate opening mechanism to generate a dam-break wave is shown in Figure 2.3. The lift gate was operated using a pulley system mechanism creating a sudden difference in water head. The gate was sufficiently open to avoid any obstruction of the generated wave. The gate is pulled up by an inextensible rope and two pulley rollers guide the rope to the side of the mechanism. A weight of 32.9 kg was used to guarantee an 'instantaneous' opening after a safety pin was removed. The gate itself slides between two 5 mm thick wooden ridges attached to the side of the flume with a contraction rate of 1:10. These were as small as possible to limit their interference with the flow. The sides and the bottom of the gate are made watertight using a kit and Silicone Grease (RS Pro) at the bottom and the sides of the gate.

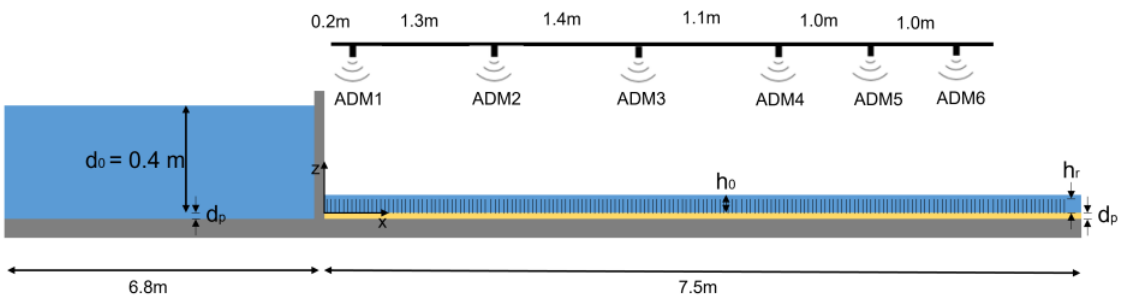

Figure 2.2: Definition sketch of the dam-break wave set-up

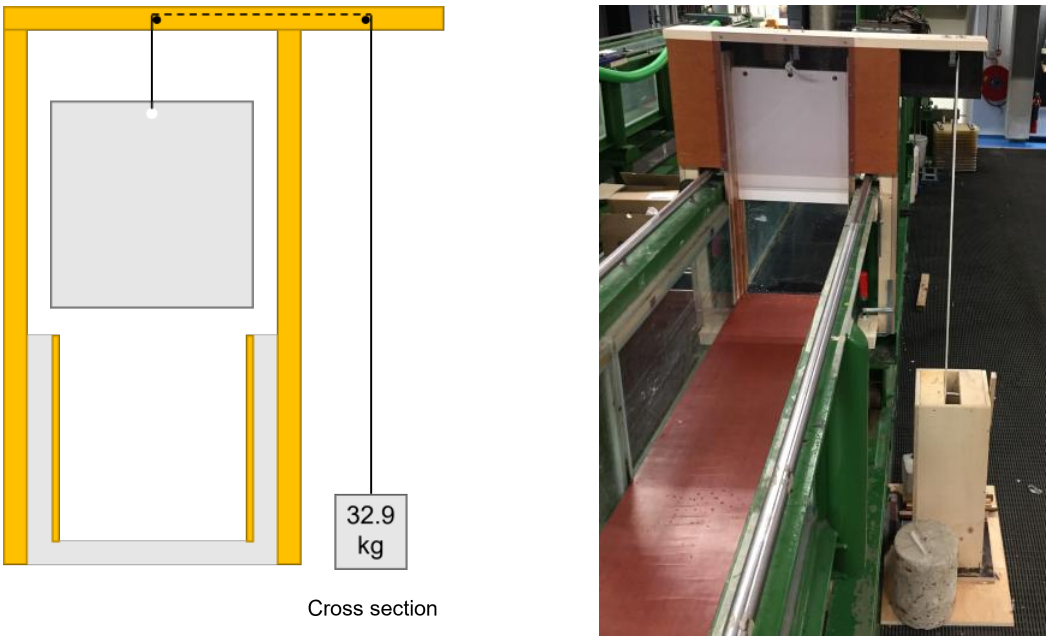

(a) (b)

Figure 2.3: Details of the gate opening mechanism

2.1.1. Instantaneous Opening of the Gate

The gate opening time is critical (Von Häfen et al., 2019). In an ideal situation, this opening should be instantaneous to generate a perfect wave. Unfortunately, this is difficult due to experimental limitations. Research by Lauber and Hager (1998a) defined opening 'instantaneous' if $t < \sqrt{2d_0/g}$ to have waves that resemble an 'ideal' dam-break downstream of the gate.
This criterion was based on the wave profile at various distances. This criterion was applied by previous research, including Aleixo et al. (2019); LaRocque et al. (2013); Leng and Chanson (2015), with opening times of about 0.1-0.2 seconds. However, research shows that this formula leads to a rather conservative time (Von Häfen et al., 2019). During the present tests the gate opening time was measured using video equipment. This resulted in an estimation of the gate opening time of 0.25 seconds, respecting the time criterion of 0.29 seconds.

2.1.2. Instrumentation

Different equipment is used to measure the hydrodynamic behaviour of the dam-break waves. These are discussed below.

- **Acoustic Displacement Meters** (ADMs) are used to measure the water depth over time at different locations within the channel (Figure 2.2). ADMs measure the required time for pulses to return to the sensor after being reflected by the first obstacle encountered.

For the first 2 configurations of dam-break tests, three Acoustic Distance Meters were used to capture the water depth over time. These three ADMs (Baumer UNAM 30I6103, Frauenfeld Switzerland) are shown with numbers 4, 5 and 6 in Figure 2.2 and are placed at 4.0, 5.0 and 6.0 meters from the gate respectively. Three additional ADMs (Microsonic ^{TM} mic+35/IU/TC, Dortmund Germany) were added for the following tests. These are numbered 1, 2 and 3 at distances 0.2, 1.5 and 2.9 meters from the gate. All ADMs were located at the channel centreline. The data was acquired with a sampling frequency of 1 kHz and the response time of the ADMs was 84 ms, an accuracy of ± 0.5 mm and the measurement range was adapted to 100-450 mm for maximum accuracy. The ADMs provide a depth averaged over a surface, of approximately 85x85 mm. The ADMs were connected to a Data Acquisition System that sampled all instruments simultaneously. By calibrating the conversion formula from Volt-values of the ADMs with a point gauge, the water depth can be determined. The data was acquired and exported into Excel files using the program DASYLab. By analysing the time of arrival of the wave tip between the different measuring points, the wave celerity was also calculated (Wüthrich et al., 2020; Xu et al., 2021).

- **Video imagery** was also used to collect information about characteristics of the dam-break wave. The digital video material can be used to support the data of the ADMs of the celerity of the wavefront (Wüthrich et al., 2020). Moreover, the wavefront profile can be analysed. Pictures and videos were taken from the side through an iPhone 6 located at 1.25 m from the glass sidewall at the location of ADM6. In order to avoid reflection, a tent of black cloths was constructed around the tripod and the flume (Figure 2.4). A black cloth was also hung behind the furthest glass panel to provide a clear background and avoid reflection. Along all sides of the front glass plate, paper rulers were installed to allow for image-based post-processing techniques. The ruler on the outside results in a small perspective error due to the thickness of the glass plate.

Pictures were also taken with a Nikon $^{(R)}$ D5500 Digital single-lens reflex camera using high shutter speed, to provide semi-instantaneous images of the propagating surges and bores.

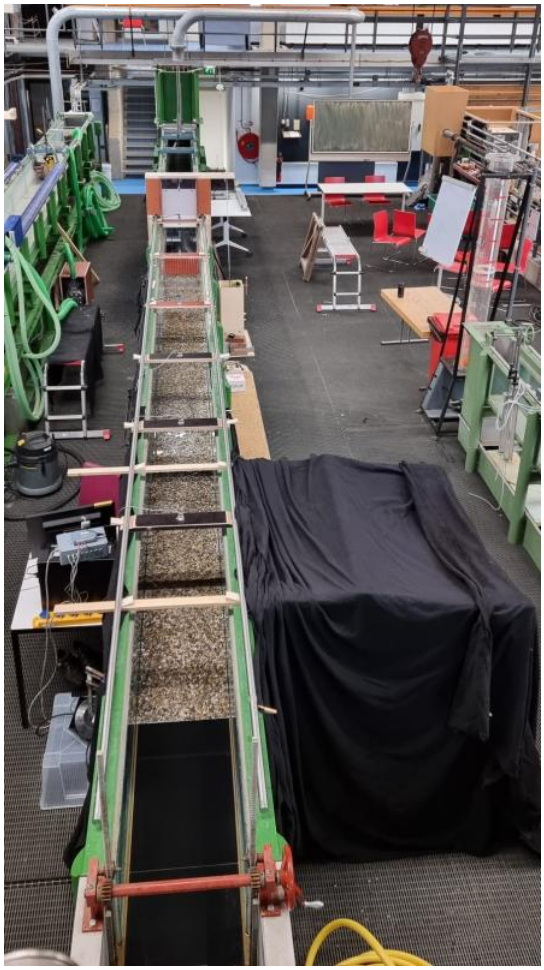

Figure 2.4: Top view dam-break wave test set-up with in the back the reservoir, halfway the flume the gate opening mechanism, in the downstream part of the flume 6 ADMs, in the front on the left side the Data Acquisition System and in the front on the right the tent for video recording and taking photos

2.2. Creating Roughness

Reference tests with a smooth bed were carried out by placing concrete plywood plates in the flume. For the tests including added roughness, two types of roughness are used with the created configurations detailed in Table 2.1 (Figure 2.5). Photos of all configurations can be found in Appendix A .

- **Wooden plates with nails** resulted in artificial bed roughness. Five different combinations of two densities and two nail heights resulted in different roughnesses. The nails were placed on a grid on the wooden plates (Table 2.1). The distance between two rows of nails was 15 or 30 mm, depending on the grid density. The rows have alternating 12 and 13 nails across the width of the plate with high-density nails. The higher density configuration was obtained by adding more nails to the low-density configurations, as detailed in Figure 2.6. Two types of nails were used: 1.6 mm diameter 25 mm length and 2.4 mm diameter 45 mm length. The 6 mm thick concrete plywood wooden plate results in effective roughness lengths of h_r = 19 and h_r = 39 mm. The location of the nails on the wooden plate was marked with a mole (see Figure 2.7), after which the holes were pre-drilled with a cordless drill using a drill bit with the same diameter as the nails. Finally, the nails were manually hammered into the 7.5 m long plates (Figure 2.8).
- **Metal plates with fixed gravel** resulted in naturally created bed roughness. Two different stone sizes were used (Table 2.1). The metal plates are 5 mm thick and the total length of 6.0 m is covered by gravel. It was decided to lay the plates from 0.70 m from the gate, with this distance covered by an artificial roughness with a similar roughness coefficient.

The small spaces between two plates were sealed with the same Silicone Grease (RS Pro) that was used to waterproof the gate. This paste prevents underflow as much as possible.
The explanation of obtaining the equivalent roughness value (k_s) for the different roughness configurations with steady flow tests is given in Appendix B.

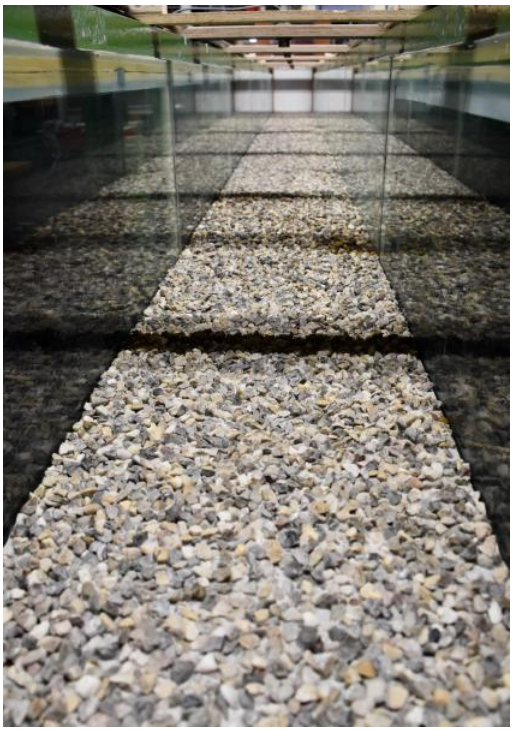

(a) Naturally created roughness R2 (large gravel d_{50} = 5 mm) k_s = 6.0 mm

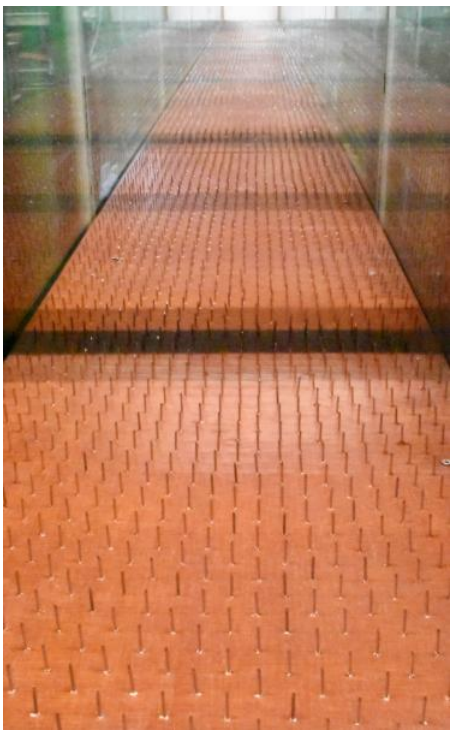

(b) Artificially created roughness R4 (small nails, high density) k_s = 10.0 mm

Figure 2.5: Roughness configurations (a) R2 k_s = 6.0 mm and (b) R4 k_s = 10.0 mm in the downstream part of the channel, seen from the end of the flume towards the gate

Roughness name	Abbreviation	Configuration	k_s (mm)
Reference	Ref	smooth	0.01
Roughness 1	R1	small gravel (d_{50} = 2 mm)	0.8
Roughness 2	R2	large gravel (d_{50} = 5 mm)	6.0
Roughness 3	R3	19 mm nails, low density	8.0
Roughness 4	R4	19 mm nails, high density	10.0
Roughness 5	R5	39 mm nails, low density	26.0
Roughness 6	R6	19 mm and 39 mm nails, high density	27.5
Roughness 7	R7	39 mm nails, high density	48.0

Table 2.1: Overview of the equivalent roughness values obtained by reconstructing the backwater curve through the measured water levels during steady flow tests (Appendix B)

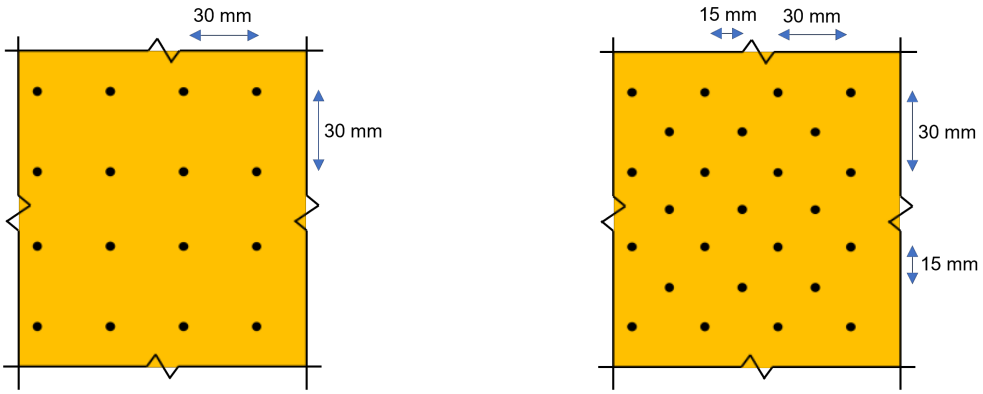

(a) Low-density grid

(b) High-density grid

Figure 2.6: Different grids and heights of nails

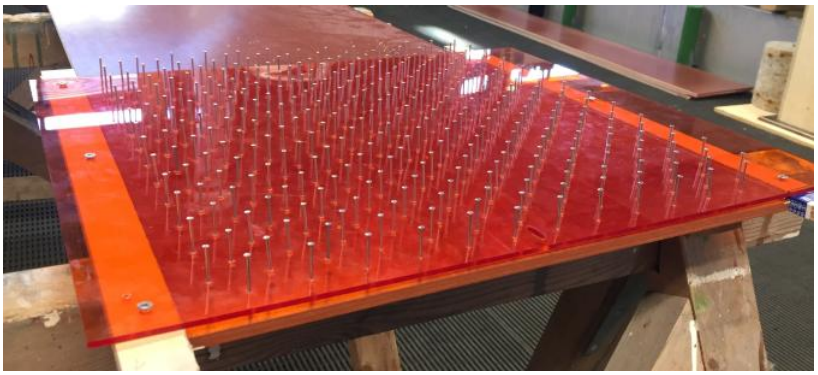

Figure 2.7: Use of a mole to apply a grid to wooden plates

Figure 2.8: Side view of artificially created roughness R7 (long nails, high density) k_s = 48 mm

2.3. Scale Effects

There are differences between a scaled model and larger prototype parameters due to model effects (incorrect reproduction of prototype features), scale effects (inability to keep each force ratio constant), and measurement effects (non-identical measurement techniques) (Heller, 2011).

Froude similarity (FM) is most often applied in literature of dam-break waves because FM is suitable for highly turbulent phenomena, where gravitational processes are dominant (Heller, 2011). Literature using FM are for example Docherty and Chanson (2010); Lauber and Hager (1998a,b); Reichstetter and Chanson (2013); Wüthrich et al. (2020). In line with literature, FM will also be used in the present study.

Scale effects do not occur if model and prototype are similar (geometric, kinematic and dynamic). This is often impossible due to economic considerations, limited time or space. Then a scaled model of scaling ration λ is, therefore, necessary and scale effects occur because not all the force ratios are identical between the real-world prototype and the model. Decreasing model size leads to increasing scale effects (Heller, 2011). The entity of scale effects depends on the parameter or phenomenon, so a presented λ value doesn't indicate whether or not scale effects can be neglected.

The common force ratio combinations in hydraulic engineering are Froude, Reynolds, Weber, Cauchy and Euler (Heller, 2011; Henderson, 1996). Froude scaling will is applied in this study with the following formula:

$$\text{Froude number (F)} = (\text{inertial force / gravity force})^{1/2} = \frac{V}{(gL)^{1/2}} \tag{2.1}$$

The scale residual effects that occur are acceptable but must be kept limited as much as possible through avoidance, compensation or correction measures (Heller, 2011). Froude modelling results in an underestimation of the Reynolds number. However, the Reynolds number must be sufficiently large to guarantee fully turbulent flow, i.e. 10^5. The Reynolds number was defined as $R = c \cdot D_H / h_0$, where c is the wavefront celerity and D_H is the hydraulic diameter using the initial still water level. Values of $5 \cdot 10^6 < R < 9 \cdot 10^6$ were obtained for all waves, which implied that a sufficient level of turbulence was ensured for both surges and bores, thus minimizing potential scale effects.

2.4. Test Protocol and Experimental Program

The dry bed tests are performed (at least) 5 times per type of roughness and reference situation, the wet bed (at least) 10 times. An overview of the experimental program with the bed condition, initial still water level, the roughness configuration, the bore Froude number, the number of measuring ADMs in the channel, the number of repetitions per type of test and the test code is presented in Table 2.2.

- The **roughness of the channel bed** was changed. All roughness configurations were tested under unsteady flow conditions and there was ensured that the bed roughness remained constant over for all the tests.
- During the tests the **initially still water level** downstream of the gate was changed. Herein a dry bed and five different still water levels were tested. The largest initially still water level (50 mm) is the maximum limit, respecting the limit $h_0/d_0 = 0.138$ imposed by Stoker (1957). Compared to previous literature, special attention is given to the very small initially water level of 7.5 mm because of the small values of k_s/h_0 (Nielsen et al., 2022).

All tests were carried out over a period of 3 months. Tests with the same combination of initially still water level and bed roughness were also conducted over several days. A squeegee and a sponge were used to speed up the drying process to guarantee reliable dry bed tests. Calibration of the ADMs was performed after installing each new roughness configuration at five different levels within the measurement range focusing on levels near the bed.

During the tests with the rough bed configurations the ADMs measured a surface affected by the nails, especially for dry bed tests. Using manual measurements it was ensured that the zero always referred to the bottom of the channel, i.e. the wooden plate used for the smooth configuration.

Bed condition	Initial water depth [h_0 (mm)]	Configuration	k_s (mm)	h_0/d_0	Bore Froude	Number of ADMs	Number of repetitions	Test code
Dry	0.0	Reference	smooth	-	-	3	9	D0R0T1-9
		Roughness 1	0.80	-	-	6	6	D0R1T1-6
		Roughness 2	6.00	-	-	6	6	D0R2T1-6
		Roughness 3	8.00	-	-	6	6	D0R3T1-6
		Roughness 4	10.00	-	-	3	5	D0R4T1-5
		Roughness 5	26.00	-	-	6	5	D0R5T1-5
		Roughness 6	27.50	-	-	6	6	D0R6T1-6
		Roughness 7	48.00	-	-	6	7	D0R7T1-7
Wet	7.5	Reference	smooth	0.01875	8.15	3	13	W7_5R0T1-13
		Roughness 1	0.80	0.01875	7.21	3	12	W7_5R1T1-12
		Roughness 2	6.00	0.01875	6.84	6	12	W7_5R2T1-12
		Roughness 3	8.00	0.01875	7.39	6	12	W7_5R3T1-12
		Roughness 4	10.00	0.01875	7.31	3	11	W7_5R4T1-11
		Roughness 5	26.00	0.01875	5.89	6	13	W7_5R5T1-13
		Roughness 6	27.50	0.01875	5.77	6	11	W7_5R6T1-11
		Roughness 7	48.00	0.01875	5.11	6	11	W7_5R7T1-11
Wet	15.0	Reference	smooth	0.0375	5.50	3	10	W15R0T1-10
		Roughness 1	0.80	0.0375	5.09	3	10	W15R1T1-10
		Roughness 2	6.00	0.0375	4.92	6	11	W15R2T1-11
		Roughness 3	8.00	0.0375	5.12	6	10	W15R3T1-10
		Roughness 4	10.00	0.0375	5.23	3	13	W15R4T1-13
		Roughness 5	26.00	0.0375	4.36	6	10	W15R5T1-10
		Roughness 6	27.50	0.0375	4.18	6	11	W15R6T1-11
		Roughness 7	48.00	0.0375	3.85	6	12	W15R7T1-12
Wet	25.0	Reference	smooth	0.0625	4.03	3	11	W25R0T1-11
		Roughness 1	0.80	0.0625	3.88	3	10	W25R1T1-10
		Roughness 2	6.00	0.0625	3.85	6	11	W25R2T1-11
		Roughness 3	8.00	0.0625	3.98	6	11	W25R3T1-11
		Roughness 4	10.00	0.0625	3.95	3	12	W25R4T1-12
		Roughness 5	26.00	0.0625	3.55	6	10	W25R5T1-10
		Roughness 6	27.50	0.0625	3.49	6	11	W25R6T1-11
		Roughness 7	48.00	0.0625	3.18	6	12	W25R7T1-12
Wet	35.0	Reference	smooth	0.0875	3.36	3	11	W35R0T1-11
		Roughness 1	0.80	0.0875	3.23	3	13	W35R1T1-13
		Roughness 2	6.00	0.0875	3.25	6	13	W35R2T1-13
		Roughness 3	8.00	0.0875	3.22	6	11	W35R3T1-11
		Roughness 4	10.00	0.0875	3.25	3	12	W35R4T1-12
		Roughness 5	26.00	0.0875	3.10	6	10	W35R5T1-10
		Roughness 6	27.50	0.0875	3.12	6	11	W35R6T1-11
		Roughness 7	48.00	0.0875	2.94	6	12	W35R7T1-12
Wet	50.0	Reference	smooth	0.125	2.74	3	11	W50R0T1-11
		Roughness 1	0.80	0.125	2.64	3	12	W50R1T1-12
		Roughness 2	6.00	0.125	2.66	6	11	W50R2T1-11
		Roughness 3	8.00	0.125	2.72	6	11	W50R3T1-11
		Roughness 4	10.00	0.125	2.66	3	11	W50R4T1-11
		Roughness 5	26.00	0.125	2.61	6	10	W50R5T1-10
		Roughness 6	27.50	0.125	2.57	6	11	W50R6T1-11
		Roughness 7	48.00	0.125	2.62	6	11	W50R7T1-11

Table 2.2: Experimental program and characteristics of the performed dam-break wave tests (the dry or wet bed condition, initial still water level, the roughness configuration, the bore Froude number, the number of measuring ADMs in the channel, the number of repetitions per type of test and the test code)

3

Methodology

This Chapter presents the way of synchronisation, filtering of the data and statistical analysis.

3.1. Data Synchronisation and Filtering

A typical result of the data that was obtained through the Data Acquisition System (DAS) can be seen in Figure 3.1. Data were checked after every test and wavefronts were synchronised to the same arrival time (t_0), as shown in Figure 3.2. This reference time is determined when the water level rises continuously by 0.01 m over 5 data points (with a total length of 5 milliseconds), without lowering the water level in those data points.

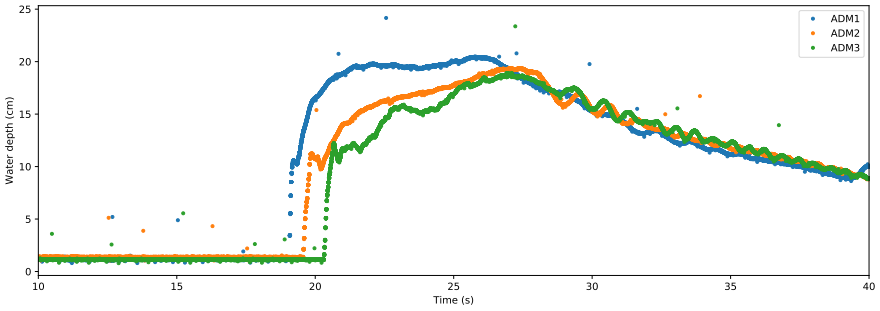

Figure 3.1: Example of unsynchronised raw water level data for ADM1,2&3 for roughness configuration R6 (k_s = 27.5 mm, combination of 39 mm and 19 mm nails), wet bed 25 mm, d_0 = 0.4 m, t = 0 is starting time data acquisition, test number W25R6T1 (Table 2.2)

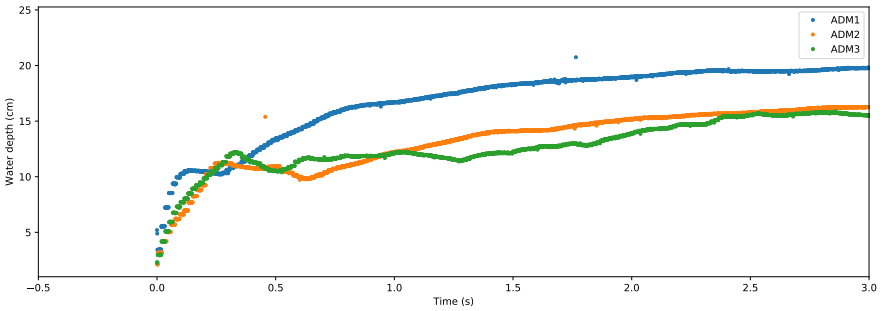

Figure 3.2: Example of synchronised raw water level data for ADM1,2&3 for roughness configuration R6 (k_s = 27.5 mm, combination of 39 mm and 19 mm nails), wet bed 25 mm, d_0 = 0.4 m, t = 0 is arrival time wave at ADM location, test number W25R6T1 (Table 2.2)

The data were filtered using a 7-point moving median filter function that removed outliers from the rest of the data. This method was used because it was able to remove multiple outliers in a row, which was not the case with a well known 3-point moving median filter function. The data were also filtered with a self-made filter function based on an outlier threshold. The filter function replaced the outliers with the average of the previous and following values in the measured range. The threshold, to determine the boundary between outliers and meaningful data, was based on the resolution of the ADMs. The effect of changing the threshold can be seen in Figure 3.3, where the number of data points in the moving median filter was increased until the difference between both filter methods was less than 1%. Data processing was stopped 20 seconds after the arrival of the wavefront at the ADM location.

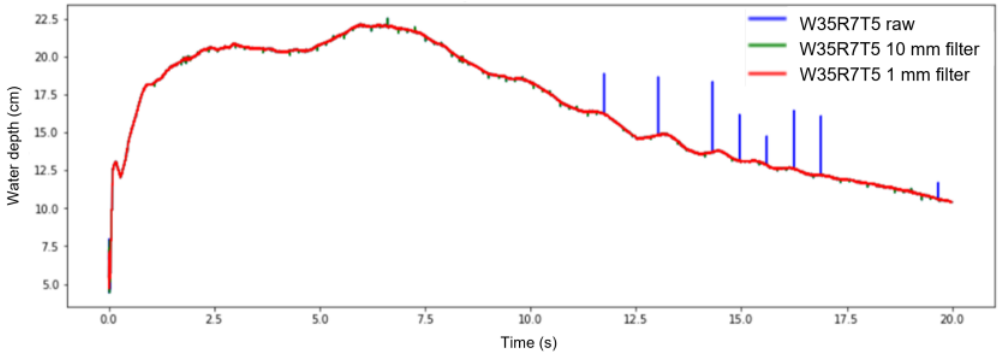

Figure 3.3: Effect of the threshold values of 1 and 10 mm for filter function on raw water level data at ADM1 (x = 0.2 m) for roughness configuration R7 (k_s = 48 mm, 39 mm nails, high density), wet bed 35 mm, test number W35R7T5 (Table 2.2)

3.2. Statistical Analysis of Unsteady Flow Data

There are mainly 3 different statistical methods that can be used to analyse data (Aleixo et al., 2019):

- **Single realization** statistics is the easiest way to come up with an average value. All data are summed and divided by the number of data points. This method can be used if the average doesn't change over the sampling period, e.g. steady flows. The sampling period could be reduced, but attention should be paid that the sampling period isn't too short (no significant data) or too long (smooth out transient effects) (Aleixo et al., 2019). This is not applicable to dam-break waves and other unsteady waves.
- **Fourier analysis** (variable interval time average or low-pass filtered) allows determining the mean value from just one run of a random transient variable. This one single realization is suitable to obtain information on instantaneous quantities qualitative patterns (Chanson, 2020). This is not applicable if the data changes a lot over time (highly unsteady wave data for example). A threshold frequency (cut-off frequency) must be calculated (Aleixo et al., 2019).
- **Ensemble statistics** uses different realizations of the same phenomenon to determine ensemble values (Aleixo et al., 2019). An ensemble average or median value of multiple runs is obtained at a specific instant (of time). A disadvantage of this method is that multiple runs must be performed, which could be critical due to time constraints, technical limitations or limited resources. An advantage is that an average value can be found for data that highly varies in time (Chanson, 2020). To choose whether the ensemble average or the ensemble median is more meaningful, it is important to look at the effect of the extreme values. When extreme data points significantly affect the result, the Ensemble Median is more suitable (Khzeri and Chanson, 2015; Leng and Chanson, 2014, 2015).

During the analysis of the dam-break wave data, both the ensemble average and ensemble median values were calculated. For the averages, the 16^{th} and 84^{th} percentiles were also calculated and for the medians, the 25^{th} and 75^{th} quantiles. These values were always calculated using the filtered individual test results. These percentiles and quantiles are in line with previous literature (Chanson, 2020; Leng and Chanson, 2017). The results differed in some situations, which showed that the ensemble median method is the most appropriate.

This ensemble median data was therefore used for further analysis of the data and generation of graphs in Chapter4 and 5.

3.3. Data Processing Parameters

Data processing is done using the synchronised, filtered data to calculate values for the four parameters describing the hydrodynamic properties that are discussed in Chapter 5. The processing is done by self-written Python scripts that were run in Jupyter Notebook.

- **Wavefront Celerity** (c)**:** For each performed dam-break wave test the travel time between two ADMs was determined by calculating the difference in arriving time of the wavefront at the ADM locations. Dividing the travel distance by the travel time resulted in the wavefront celerity between these two ADMs. For one type of test with a specific roughness configuration and initially still water level the median of the multiple wavefront celerities was taken. This results in 5 wavefront celerities over the channel. For processing of the celerities, it was assumed that the wavefront celerity was constant between two ADMs. After the wave is developed, this assumption is in line with theory presented by Stoker (1957). In addition, the wavefront celerity based on the side view videos was calculated by analysing the interval time between two frames for a known travel distance.

- **Maximum Wave Height** (h_{max})**:** For each performed dam-break wave test the maximum wave height was calculated by finding the maximum measured water level over the acquisition period that was not affected by a potential reflection wave. For one type of test with a specific roughness configuration and initially still water level the median of the maximum wave heights was used for the analysis.

- **Plateau Height** (h_2)**:** To calculate the plateau height, its duration was determined first. The start and end time of the plateau was identified by taking the first derivative of the water depth over time and looking for derivatives close to zero. The first value smaller than 5% of the previous derivative value in absolute terms was accepted as the start time of the plateau. The first value that was larger than 5% of the previous one resulted in the end time. The average water level over this plateau duration was calculated and used as plateau height. The presence of a plateau height and the calculated height were visually checked by plotting the water depths over time, including the calculated plateau height highlighted.

- **Roller Length** (L_r)**:** The roller length was calculated by multiplying the roller time by the wavefront celerity of the wave measured between ADM5 and ADM6. This was only done for test configurations where a plateau height was present. The roller time was obtained by determining the time interval between arrival of the wavefront and the moment the first derivative of the water depth was smaller than 5%. Its determination by analysing the moment when the water depth equals the plateau height was not preferred here because it resulted in an overestimation of the roller time. The roller length was also checked with video analysis, which showed consistency with the approach used herein.

4

Visual Observations and Validation

This Chapter presents and discusses the visual observations of the dam-break wave tests and validation of the dam-break wave facility against previous studies available. The data obtained during this project can be found at `https://www.doi.org/10.4121/20017565`.

4.1. Visual Observations Dam-Break Wave Tests

Visual observations allow for a better interpretation of the results derived from this experimental project. The observations are presented from upstream to downstream of the channel, starting at the gate. The water level in the reservoir was checked manually and a constant water level was observed, meaning that the water was at rest. There was visually checked that no leakage occurred at the downstream part of the gate to make sure the channel was kept dry or the initially still water level was kept constant before data acquisition was started. When the gate was opened, the 0.4 m water level reservoir was released into the channel with dry, wet, smooth or rough bed. Because of the initial resistance of the channel bed, a breaking process was seen in the flume, as shown in Figure 4.1 and the dam-break wave started to develop.

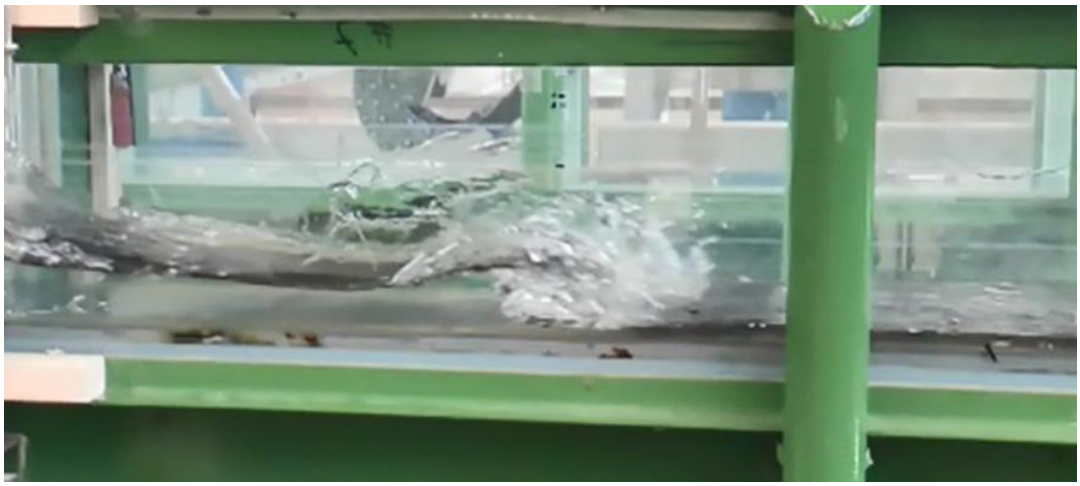

Figure 4.1: Breaking bore after releasing the water from the reservoir into the downstream channel 0.7 m downstream of the gate for a Ref (smooth) wet bed 25 mm test (flow from left to right), test W25R0T9 (Table 2.2)

A substantial difference in wavefront behaviour was observed during the flow in the downstream channel between dry bed surges and wet bed bores, in line with previous literature (Wüthrich et al., 2018, 2019). The dry bed surges showed a more constant rise in water level without any breaking. The wet bed bore had a more turbulent front characterized by strong aeration and a steeper bore front slope, as shown in Figure 4.2, taken at ADM6 (x = 6.0 m). This Figure presents the side view of three different bore fronts, where some features associated with Strong Free-Surface Turbulence previously identified by Wüthrich et al. (2021) are

visible (Figure 4.2c). This turbulence is accompanied by air entrainment in the bore front and breaking is clearly visible through the glass sidewalls, see the difference between Figures 4.2b and 4.2c. The front view of the wave supports the observations of the increase of turbulence for increase of the initially still water level of the side views, see the difference between Figures 4.5a and 4.5b for R1 (k_s = 0.8 mm) configurations and Figures 4.4a and 4.4b of R7 (k_s = 48 mm) configurations.

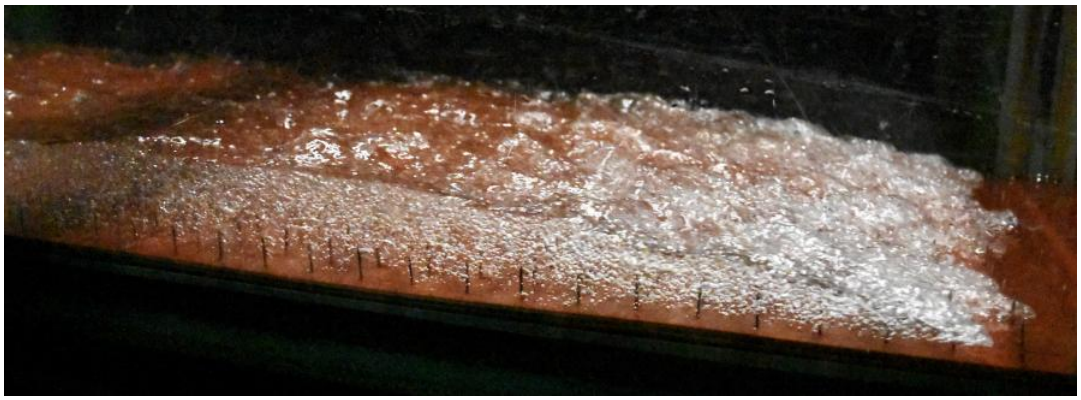

(a)

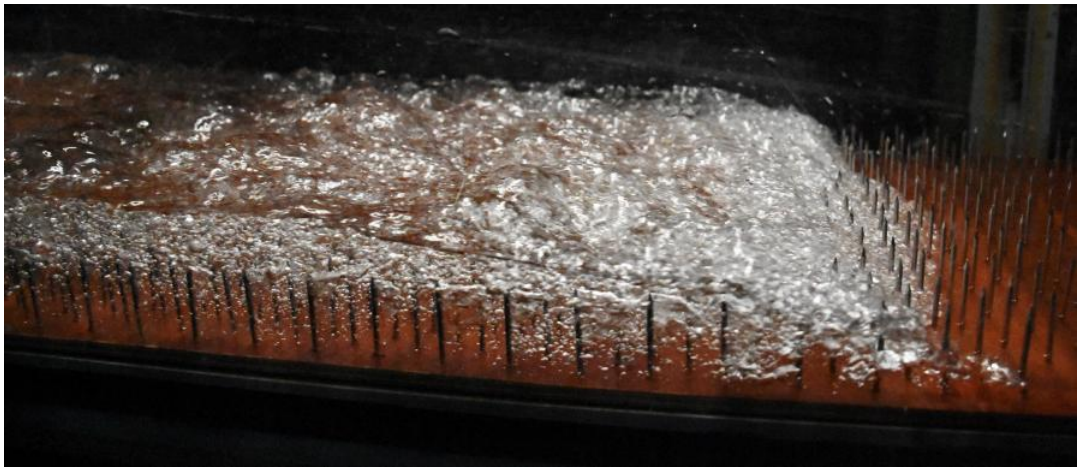

(b)

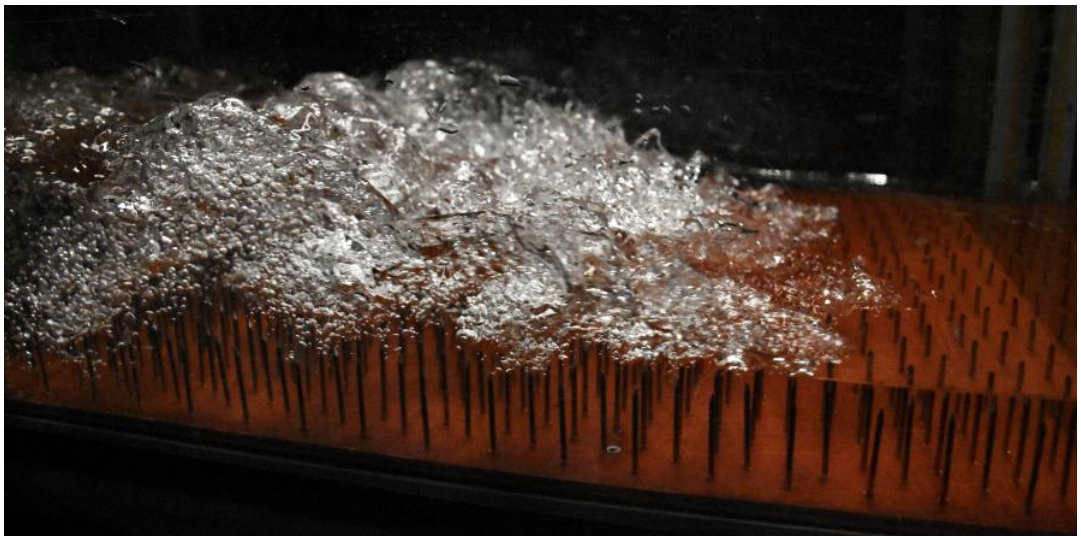

(c)

Figure 4.2: Side views of arrival of bores for (a) R3 (k_s = 8.0 mm) 7.5 mm wet bed, (b) R7 (k_s = 48 mm) 7.5 mm wet bed and (c) R7 (k_s = 48 mm) 50 mm wet bed tests at x = 6.0 m (flow from left to right) (Photos: Davide Wüthrich)

(a) (b)

Figure 4.3: Comparison of front view of wavefronts of (a) a dry bed surge and (b) a wet bed bore (50 mm) for small gravel roughness configuration R1 (k_s = 0.8 mm) (flow from back to front) (Photos: Davide Wüthrich)

In dry bed and wet bed tests where the initially still water level is below the top of the nails ($h_0 < h_r$), air bubbles were seen along the nails when the wave passed by. This occurrence was best visible near the gate but was present throughout the flume length (Figure 4.2b). Several wet bed bores showed a sudden increase in water height, followed by a relatively long and constant water height, the plateau at ADM6. The start of a plateau can be seen in Figure 4.2b.

Figures 4.2a and 4.2b show wavefronts of 7.5 mm wet bed tests of roughness configuration R3 (k_s = 8 mm) and R7 (k_s = 48 mm). A higher bed roughness seems to lead to a steepening of the wavefront and an increase in turbulence and air-entrainment in the wave. This is supported with front views of the waves in Figures 4.5a and 4.5b showing dry bed tests of R3 (k_s = 8 mm) and R7 (k_s = 48 mm) configurations. In Figure 4.4b some slugs, S-shaped cords of foamy mixture (Wüthrich et al., 2021), can be seen, showing consistency with previous studies. The combined influence of initially still water level and bed roughness on dam-break waves for several configurations can be seen in Figure 4.6.

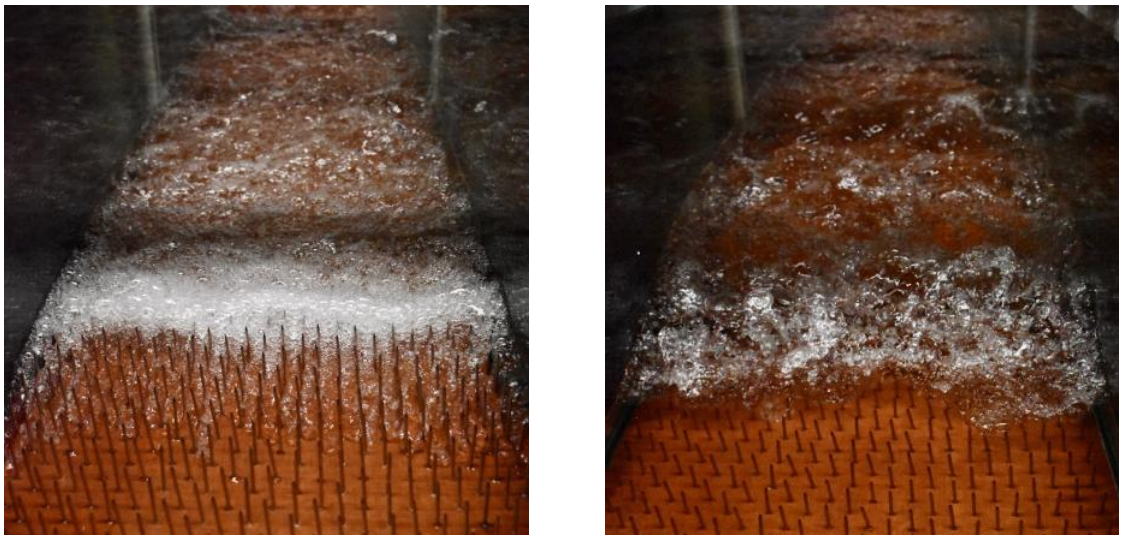

(a) (b)

Figure 4.4: Comparison of front view of wavefronts of (a) a R7 (k_s = 48 mm) dry bed and (b) a R7 (k_s = 48 mm) 50 mm wet bed (flow from back to front) (Photos: Davide Wüthrich)

(a) (b)

Figure 4.5: Comparison front view of wavefronts of a dry bed surges for (a) a R3 (k_s = 8 mm) roughness bed and (b) a R7 (k_s = 48 mm) bed roughness bed (flow from back to front) (Photos: Davide Wüthrich)

A reflection wave from the downstream sill (x = 14.0 m) can be seen from R1 (k_s = 0.8 mm) until R4 (k_s = 10 mm) with a 50 mm initial still water level. A comparison of two time moments during the test for one of these configurations is shown in Figure 4.7. The bore travels from left to right, indicated by the blue arrows, and the return wave flows from right to left, indicated by the red arrow. This reflection wave could be explained by the limited outflow capacity at the end of the flume. For larger roughness values, this reflected wave is no longer visible.

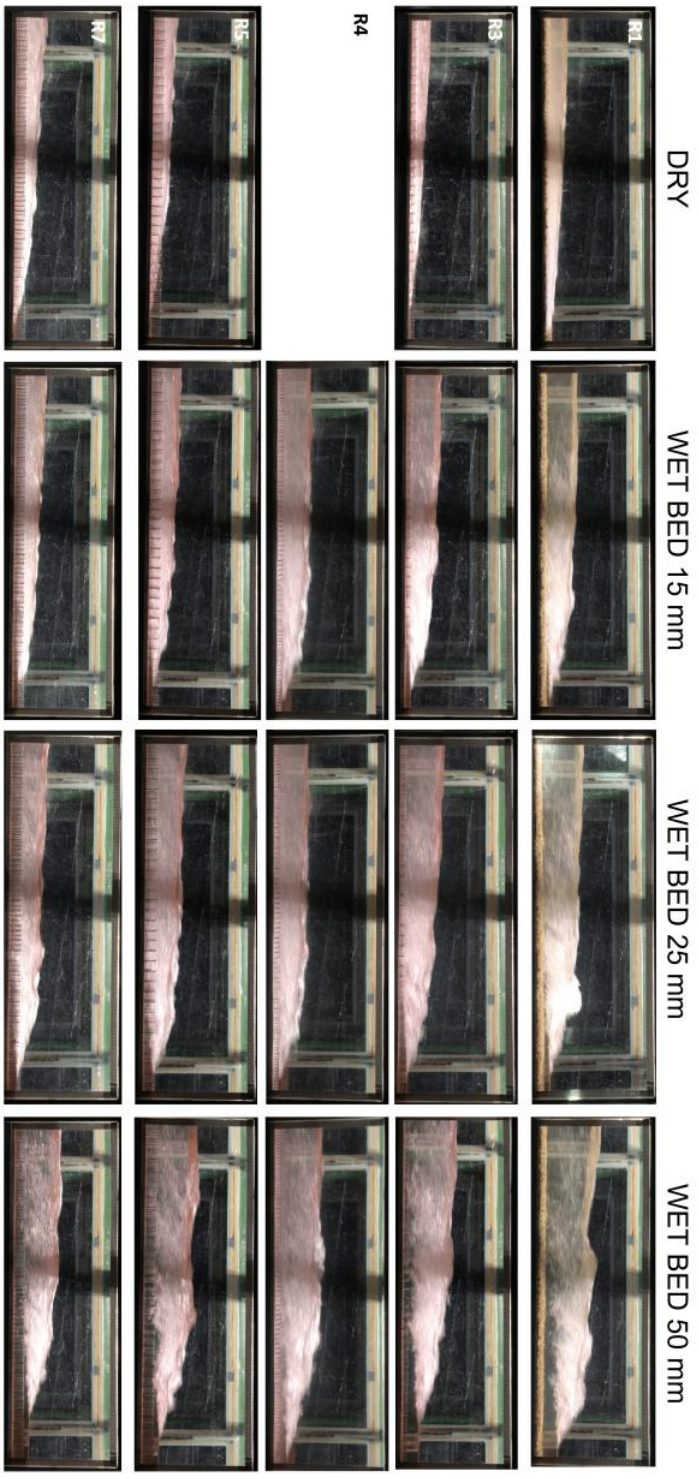

Figure 4.6: Overview of side view wavefronts for dry and wet bed (15, 25 and 50 mm) tests for roughness configurations R1 (k_s = 0.8 mm), R3 (k_s = 8 mm), R4 (k_s = 10 mm), R5 (k_s = 26 mm) and R7 (k_s = 48 mm). A side view video of the dry bed R4 (k_s = 10 mm) test is missing (flow from left to right)

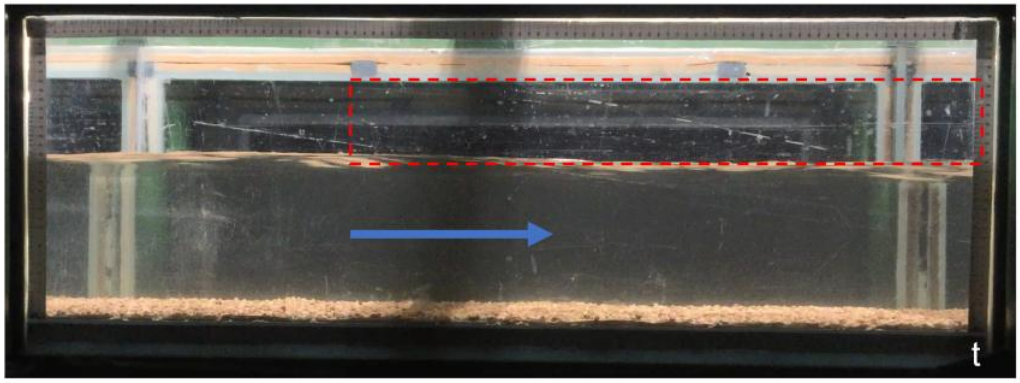

(a)

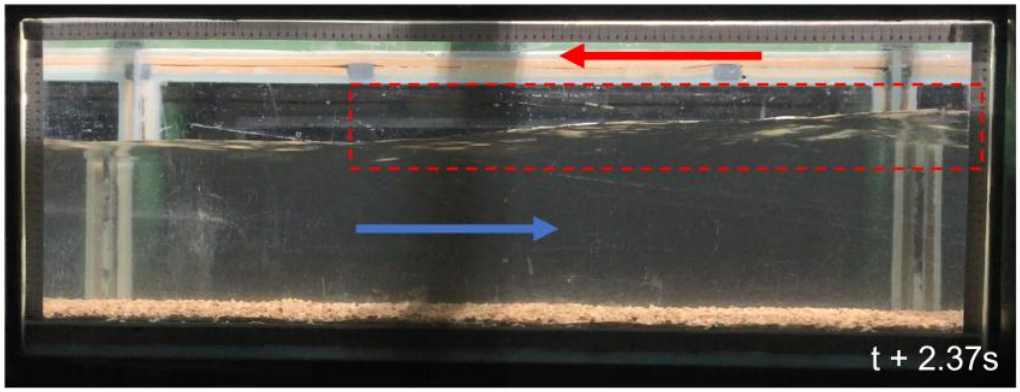

(b)

Figure 4.7: Comparison of side views of dam-break wave at (a) time t and (b) time t+2.37s to show reflection at end of the flume. A wet bed 50 mm bore traveling over roughness configuration R1 (k_s = 0.8 mm) (bore flows from left to right, indicated by blue arrow; reflection wave flows from right to left, indicated by red arrow)

4.2. Validation of Smooth Bed Surges and Bores

This Section will validate the surges and bores generated with the dam-break wave facility on smooth beds against existing literature and previous studies available in literature. The main parameters used in the validation and presentation of the results are defined in Figure 4.8 where a ensemble median result of a 50 mm wet bed bore on a R2 (k_s = 8 mm) bed configuration can be seen.

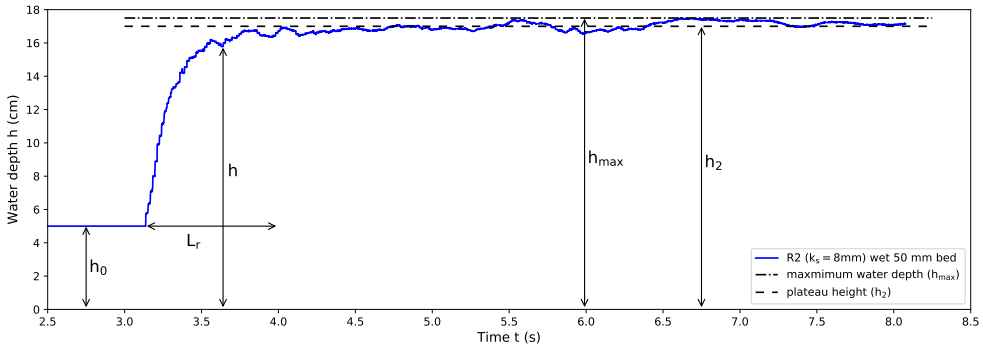

Figure 4.8: Definition of main variables of the dam-break wave results on a ensemble median result of a 50 mm wet bed bore on a R2 (k_s = 8 mm) bed configuration

To validate the measured data and make sure that tests conducted herein are aligned with existing theories and literature, the water level of the smooth, dry bed surges are compared to Ritter's (1892) theory and the smooth, wet bed bores are compared to Whitham's (1955) theory. Only three measurement locations downstream of the gate were used for the comparison where the wave was fully developed. At the time of the dam-break wave's arrival at ADM6, the water levels at ADM4 and ADM5 were extracted, resulting in the first three data points (combinations of ADM locations and arrival time at ADM6) in the Figures 4.9 and 4.10, which corresponded to an instantaneous "screenshot" of the propagating wave.

To obtain more data points along the theory line of Ritter (1892) water levels were extracted in a time zone just before and after the wavefront tip arrival at ADM6 as shown in Figures 4.9 and 4.10. Using this new approach, it reconstructs a semi-instantaneous profiles of the water level over the entire longitudinal axis of the flume, based on only three measurement points (ADMs). The generation of more data points can only be done under the assumption that the wave travels with constant speed and has a quasi-constant shape. To meet these conditions the water level must be still in the rising part of the wave, therefore data generation is only done for 0.25 seconds before and after arrival of the wave at ADM6. The quasi-steady shape of the bore front during the rising time was checked with the side view videos. The wave speed is approximately equal to the wavefront celerity, as previously shown by Wüthrich et al. (2018).

Figure 4.9 shows that the ensemble median results of all the smooth, dry bed surges, are consistent with Ritter's (1892) theory. The small deviations between Ritter's theory and the data observable at the wave tip zone ($1.1 < x/(t \cdot \sqrt{gd_0}) < 1.4$) are due to the fact that the reference bed configuration is not completely smooth but has a very small roughness, resulting in the bull-nose shape predicted by the theory of Whitham (1955),Dressler (1952) and Chanson (2006a).

Figure 4.10 presents the smooth, 50 mm wet bed bores, showing that the results are consistent with Whitham's (1955) theory for smooth, wet bed configurations. A clear plateau height is visible for the smooth, wet bed test, as predicted by the theory of Stoker (1957) and shown in Figure 1.6. Moreover, the water levels during the rising period after the arrival of the wavefront are consistent with Whitham's (1955) theory.

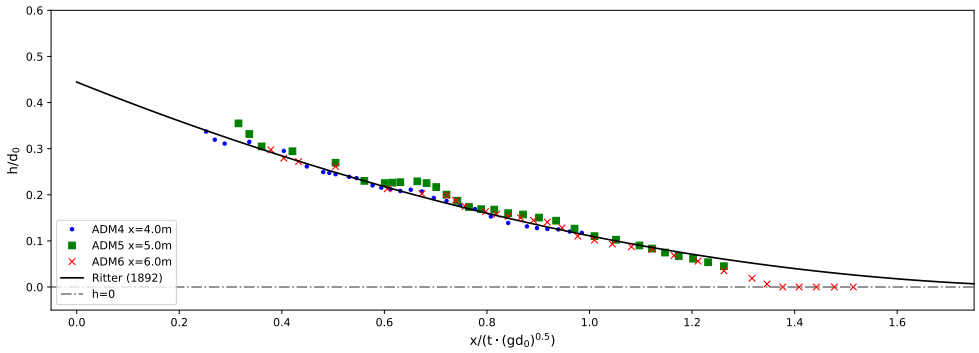

Figure 4.9: Longitudinal dimensionless water surface profiles when the wave reached measurement locations ADM4,5&6; comparison roughness configuration Ref (smooth bed), dry bed with d_0 = 0.40 m with the theoretical solutions from (Ritter, 1892)

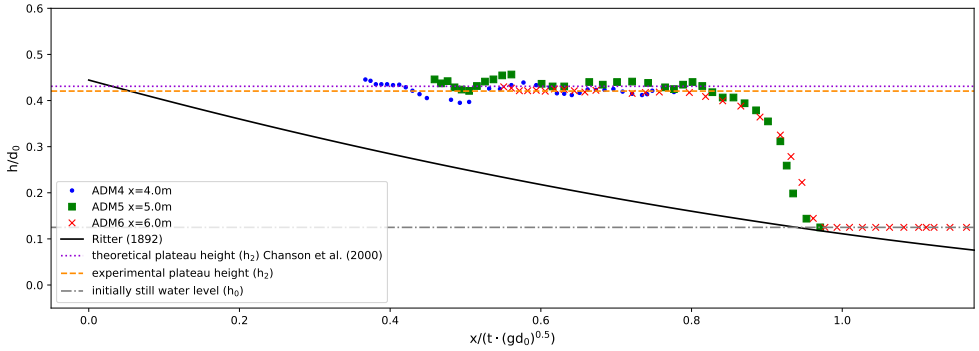

Figure 4.10: Longitudinal dimensionless water surface profiles when the wave reached measurement locations ADM4,5&6; comparison roughness configuration Ref (smooth bed), wet bed 25 mm with d_0 = 0.40 m with the theoretical solutions from (Ritter, 1892)

4.3. Validation of Surges and Bores over Additional Bed Roughness

This Section will validate the surge and bore set-up for tests on beds with added roughness.
Stoker's (1957) theory predicts that the breaking wave reaches a quasi-steady flow condition after a certain "development time" and then the wave can be considered as a shock wave. This condition was also encountered by Nielsen et al. (2022). Here it is verified if the dam-break waves generated in the present set-up also reached this quasi-steady flow condition i.e a constant wavefront celerity, in line with previous experiments. For all tests, the development length was determined by analysing the wavefront celerity over the downstream flume, with the ensemble median result presented in Figure 4.11, where one can note that a constant wavefront celerity is reached after $x/d_0 = 9$. The data is successfully compared to measurement data from Nielsen et al. (2022) and Stoker's (1957) and Ritter's (1892) theory.

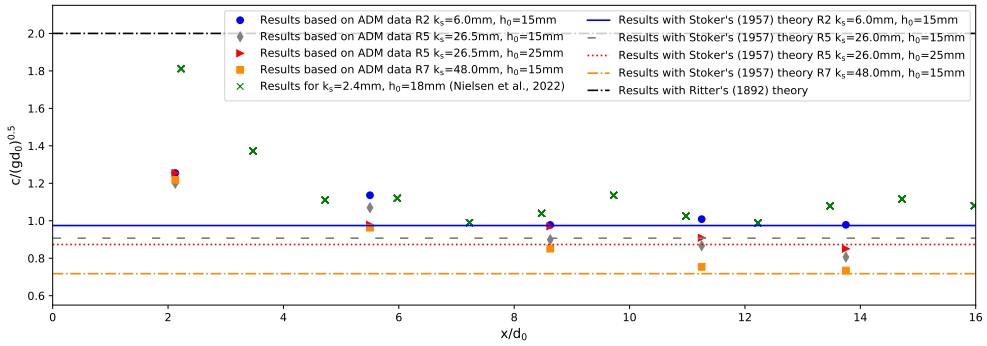

Figure 4.11: A comparison of ensemble median dimensionless wavefront celerities over downstream flume with data of Nielsen et al. (2022), Stoker's (1957) and Ritter's (1892) theory for roughness configuration R2 (k_s = 6.0 mm, wet bed 15 mm), R5 (k_s = 26.0 mm, wet bed 15 and 25 mm), R7 (k_s = 48.0 mm, wet bed 15 mm)

The longitudinal development of the wavefront celerity over the downstream flume can be seen in Figure 4.12. For all rough configurations, the wavefront celerity was quasi-steady at ADM4 (reaching an asymptotic value), which means that the generated dam-break waves have reached the quasi-steady flow conditions and can therefore be considered fully-developed, thus a shock wave.

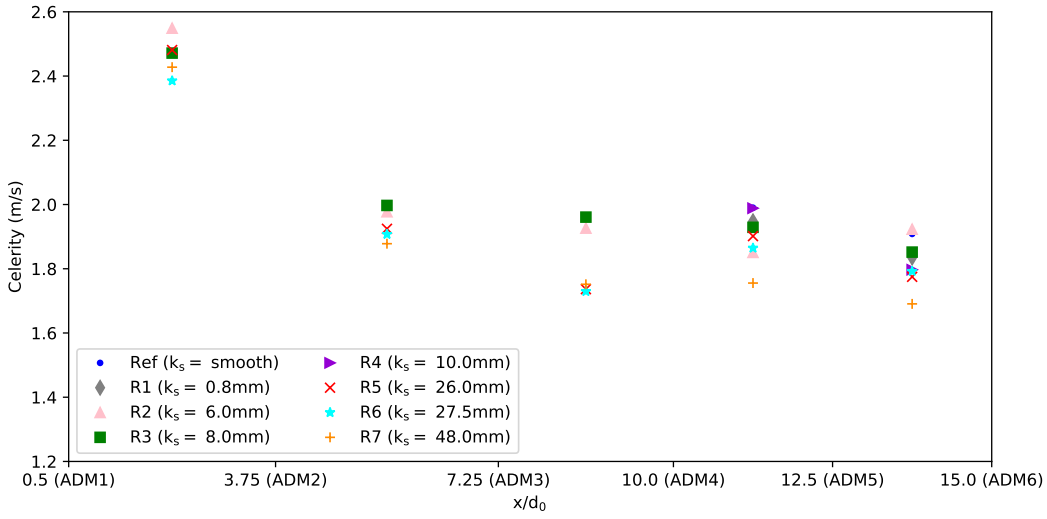

Figure 4.12: Comparison of ensemble median wavefront celerity over downstream flume for several roughness configurations for wet bed 35 mm tests, d_0 = 0.4 m

Nielsen et al. (2022) suggested that the development length (L_x) was a function of the bed roughness, suggesting the empirical expression in Equation 1.12. The development lengths of all roughness configurations were compared to the formula by Nielsen et al. (2022) in Figure 4.13, showing relatively good agreement.

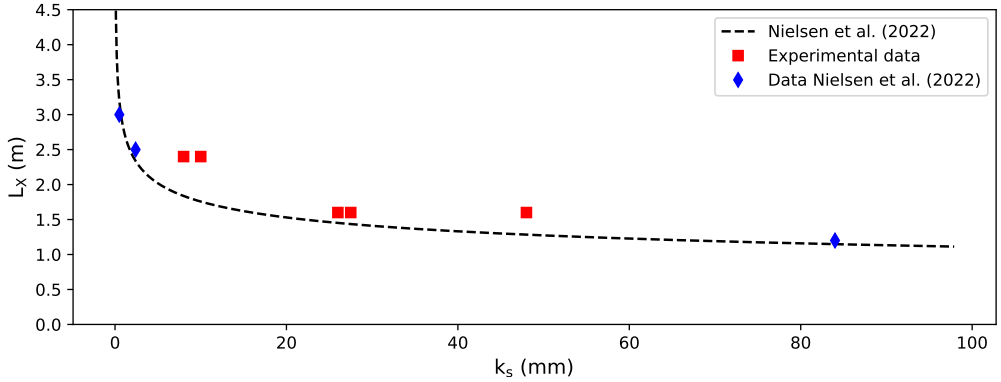

Figure 4.13: Development lengths for several bed roughness configurations compared to the data and formula (Eq. 1.12) provided by Nielsen et al. (2022)

In addition to the wavefront celerity, the maximum wave height and the plateau height show also to have reached a quasi-steady condition when the wave is developed and therefore can be considered as a shock wave. The maximum wave height over the downstream flume length is shown in Figure 4.14. The maximum water levels are compared to the most downstream measured maximum water level at ADM6. The maximum wave height increases with bed roughness, however, is quasi-steady over the flume length.

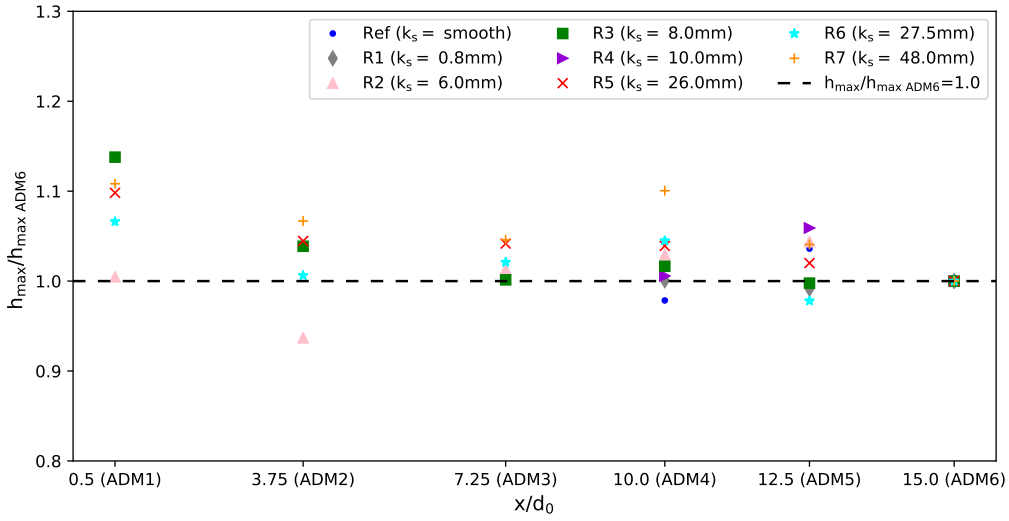

Figure 4.14: Ensemble median maximum water levels (h_{max}) over downstream flume length for several roughness configurations, wet bed 25 mm. The maximum water levels are compared to the most downstream measured maximum water level of their roughness configuration at ADM6

The plateau height (h_2), when observed, over the downstream flume length for different roughness configurations for a wet bed 50 mm test is shown in Figure 4.15. Although the plateau height decreases over the flume length, it reaches a quasi-steady value after the wave is developed, i.e. downstream of ADM4.

In Sections 4.2 and 4.3 the validation of the results for smooth and rough bed tests was described. The dry, smooth bed surges were consistent with Ritter's (1892) and Whitham's (1955) theory and the wet, smooth bed bores were consistent with Whitham's (1955) and Stoker's (1957) theory. The rough bed results showed quasi-steady wavefront celerities, maximum water levels and plateau height from ADM4 ($x/d_0 = 10.0$) on confirming that the wave is well developed, thus can be seen as a shock wave, at ADM6 ($(x/d_0 = 15.0)$. To conclude, the results of the dam-break waves generated with the facility of the present study were consistent with theory.

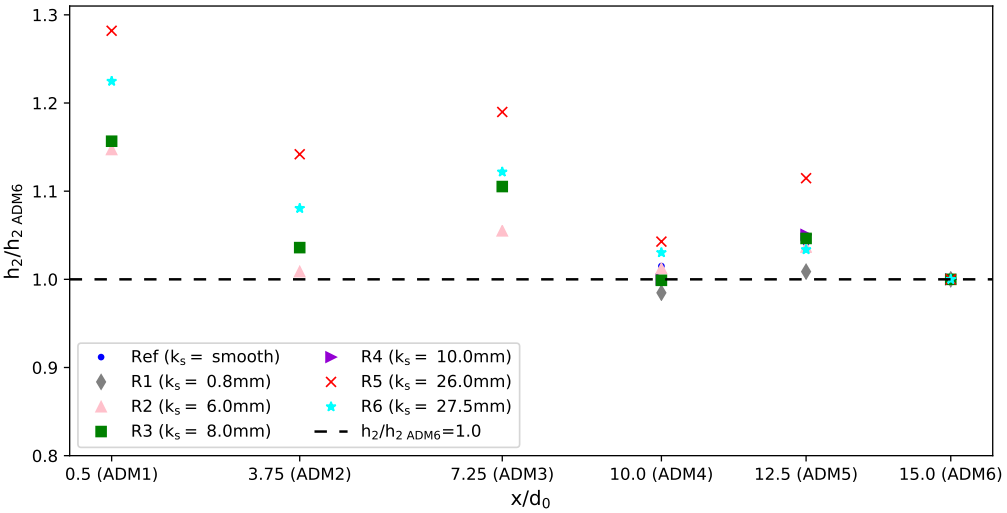

Figure 4.15: Ensemble median plateau heights (h_2), if observed, over downstream flume length for several roughness configurations, wet bed 50 mm. The plateau heights are compared to the most downstream measured plateau height at ADM6

5

Results and Analysis

After it was shown that the generated waves are consistent with previous studies and theories on dam-break waves, the influence of bed roughness and initial still water level on the results for the four parameters (c, h_{max}, h_2 and L_r) describing the hydrodynamic properties of the dam-break wave are presented and analysed in the following sections. First, several typical time evolutions of the dam-break waves are presented in Figures 5.1, 5.4 and 5.5. The tests were performed according to the described experimental program with the described test set-up of Chapters 2.1 and 2.4.

5.1. Time Evolutions of Surges and Bores

Figure 5.1 shows the ensemble median time evolution of dry bed surges with different roughness configurations at ADM6. At t=0, the gate is opened and the reservoir volume is released into the downstream part of the flume, where ADMs measure the water depths at various locations. Results show that a change in bed roughness leads to different arrival times (hence different wavefront celerities), suggesting that for dry bed surges an increase in bed roughness results in a delay of the wavefront arrival. Figure 5.1 also suggests that the steepness of the rising part of the wave and the absolute water levels increase with increasing bed roughness, changing the maximum water level parameter per configuration.

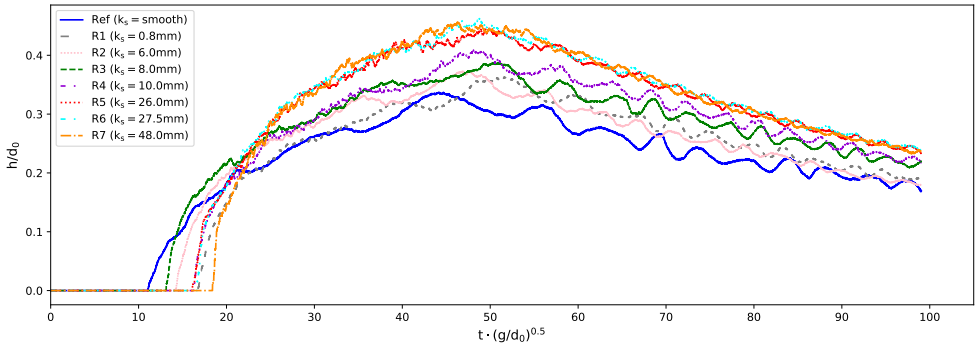

Figure 5.1: Ensemble median time evolution of dry bed surges (d_0 = 0.4 m) with different roughness configurations at ADM6 with t=0 is the opening time of the gate at x=0

Figure 5.2 shows the time evolution of the ensemble median water level and the measured at ADM6 (x = 6.0 m) for a selection of roughness configurations Ref (smooth), R3 (k_s = 8 mm), R5 (k_s = 26 mm) and R7 (k_s = 48 mm) presented in Figure 5.1. The arrival of the surges at ADM6 (x = 6.0 m) is synchronised to facilitate comparison of the water depths over time and the same trend of increasing water levels for increasing bed roughness is seen. Next to the behaviour of the water depth over time for a wide range of ks values, it suggests that the 25^{th} and 75^{th} quantile fluctuations are affected on bed roughness. The fluctuation around the

median for all test configurations for the rising time of the water level is determined by calculating the Root Mean Square Error (RMSE) for the water level range (25^{th} and 75^{th} quantile) around the median, resulting in Figure 5.3. An increase in fluctuations around the median can be noticed for an increase in bed roughness, especially in the rising part of the surge. Although at least 5 dry bed tests are performed per configuration compared to at least 10 for wet bed tests, the fluctuations for dry bed tests are relatively small compared to the other configurations.

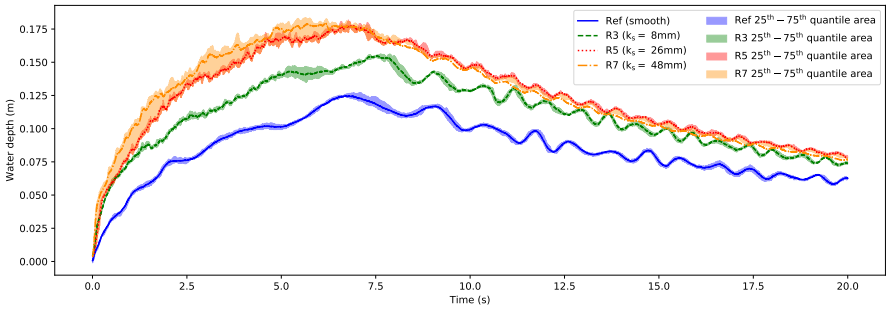

Figure 5.2: Time evolution of the ensemble median dry bed surges over acquisition period at ADM6 (x = 6.0 m) with d_0 = 0.4 m for roughness configurations Ref (smooth), R3 (k_s = 8 mm), R5 (k_s = 26 mm) and R7 (k_s = 48 mm). The area enclosed by the 25^{th} and 75^{th} quantiles are shown for the ensemble median water level results

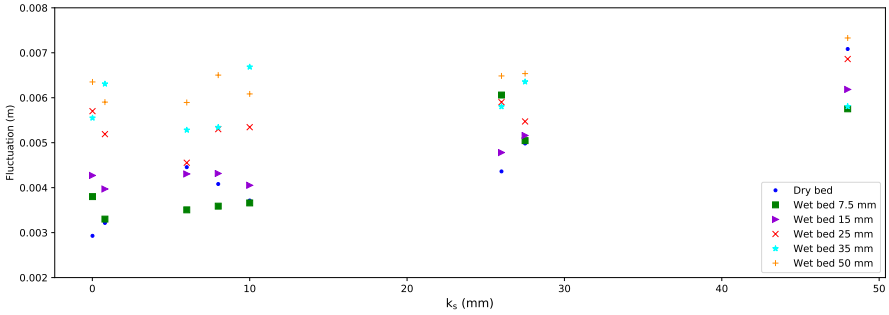

Figure 5.3: The influence of bed roughness on the fluctuations (RMSE of the 25^{th} and 75^{th} quantile) around the median water depth during the rising part of the wave for dry, wet, smooth and rough bed tests at ADM6 (x = 6.0 m) with d_0 = 0.4 m

Figure 5.4 shows the ensemble median time evolution of a dry bed surge and wet bed bores for the reference (smooth bed) configuration at (x = 6.0 m). For a smooth bed, increasing the initially still water level leads to a delay in the arrival of the wavefront and reduces the speed at which the water level rises which results in an increase in roller time. For larger tailwaters ($h_0/d_0 > 0.0625$) the absolute plateau height increases with increasing tailwater.

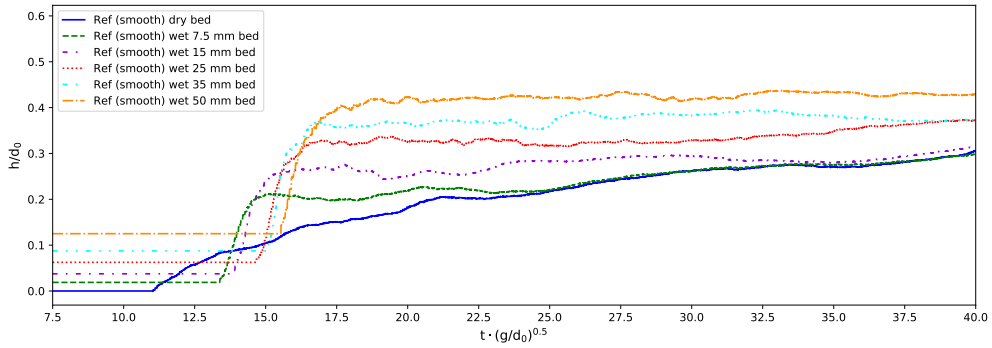

Figure 5.4: Ensemble median time evolution of dry bed surges and wet bed bores (d_0 = 0.4 m) with roughness configuration Ref (smooth) and different initially still water levels at ADM6 with t=0 is opening time of the gate at x=0

The time evolution of the ensemble median water depths for a wet bed bore (h_0 = 0.0075 m) with roughness configuration R5 (k_s = 26 mm) at different locations along the channel is shown in Figure 5.5, where x = 0 is the location of the gate. It can be noticed that a plateau is visible near the gate, but this disappears in the downstream part, where the propagating bore becomes fully developed and the maximum water depth decreases along the channel.

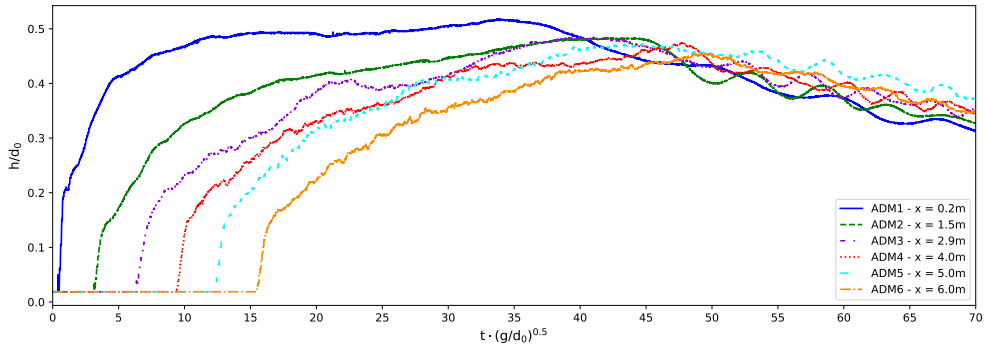

Figure 5.5: Ensemble median time evolution of a wet bed bore (d_0 = 0.4 m, h_0 = 0.0075 m) with roughness configuration R5 (k_s = 26 mm) at different locations along the longitudinal axis of the downstream channel, x = 0 is gate location

The typical time evolutions of the dam-break waves in Figures 5.1, 5.4 and 5.5 have shown that the wavefront celerity, maximum water level, the plateau height and the roller length are influenced by bed roughness and initial still water levels, therefore the influences on these parameters with be presented in the following Sections.

5.2. Effect of Bed Roughness on Wavefront Celerity

The effect of bed roughness on the wavefront celerity is presented in Figure 5.6, where it can be noted that a higher roughness is associated with a lower wave celerity. This was consistent for both data measured with ADMs and video analysis, despite the fact that the latter had a larger margin of error due to the limited number of frames available per second. For dry bed surges, the wavefront celerity was decreased with 49% for R7 (k_s = 48 mm) compared to the Reference bed (smooth). The wet bed bores show the same trend, although the reduction in celerity is smaller, with reductions in the range of 37 to 4% going from $\sqrt{h_0}$ = 7.5 mm to $\sqrt{h_0}$ = 50 mm. The side view videos confirmed the results of the ADMs. An overview of the results and differences between the celerities obtained with the ADMs and videos can be found in Appendix C. The effect of the initially still water level on the celerity that can be seen in Figure 5.6 will be discussed in Section 5.3.

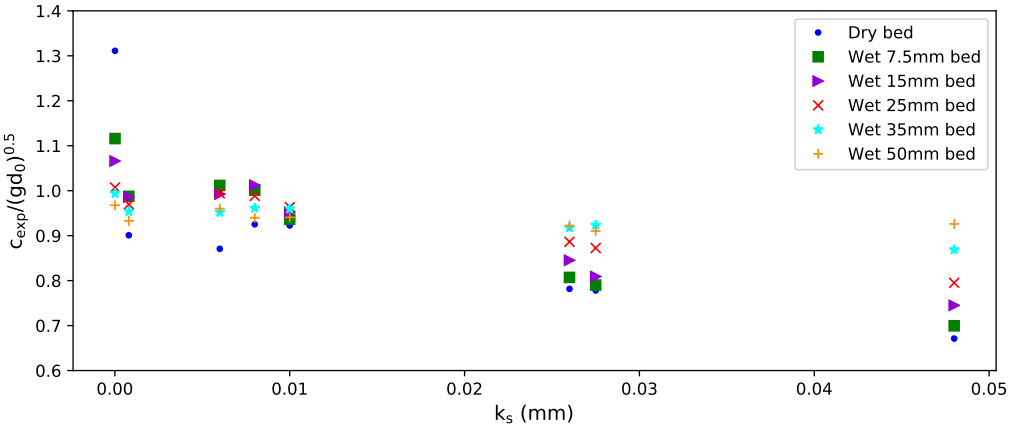

Figure 5.6: The influence of bed roughness on the ensemble median wavefront celerities for several dry and wet bed configurations, normalised using the typical celerity $\sqrt{gd_0}$ for test with d_0 = 0.4 m at ADM6 (x = 6.0 m)

Figure 5.7 shows some ensemble median wavefront celerities of dry and wet bed tests compared to previously performed studies, expressed in the form of Equation 1.13. Previous studies mostly used experimental tests to derive the best α values for their wavefront celerities, although the test conditions were different.
The result of the roughness configuration Ref (smooth), dry bed tests of the present study found the best correlation with results between studies of Kirkoz (1983) ($\alpha = \sqrt{2}$) and Wüthrich et al. (2018) ($\alpha = 1.25$). The result of R3 (k_s = 8.0 mm), dry bed has the best fit with the $\sqrt{gd_0}$ line ($\alpha = 1$). The dry bed roughness configuration R7 (k_s = 48 mm) had the best fit with Matsutomi and Okamoto (2010) ($\alpha = 0.66$). The celerities of 50 mm wet bed tests with roughness configurations Ref (smooth), R3 (k_s = 8.0 mm), R7 (k_s = 48 mm) are comparable to the $\sqrt{gd_0}$ theory ($\alpha = 1$). For dry bed surges, the wavefront celerities decrease for an increase in roughness and lead to better fits with a smaller α values, as shown in Figure 5.8. This shows a clear dependence of the wavefront celerity on both roughness and initial still water level that will be further developed in the next sections.

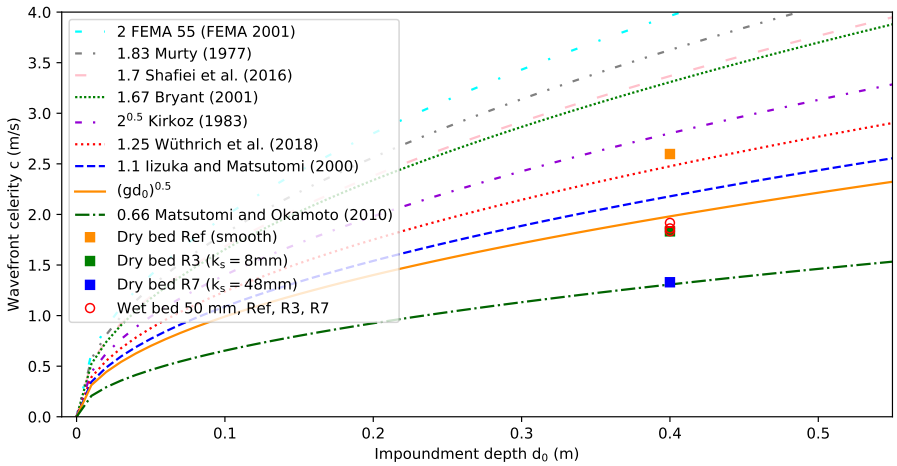

Figure 5.7: A comparison between experimental obtained ensemble median wavefront celerities and in theory presented wavefront celerities for several α values for various dry and wet bed configurations for increasing reservoir depths. References: Bryant (2001); FEMA (2001); Iizuka and Matsutomi (2000); Kirkoz (1983); Matsutomi and Okamoto (2010); Murty (1977); Shafiei et al. (2016); Wüthrich et al. (2018)

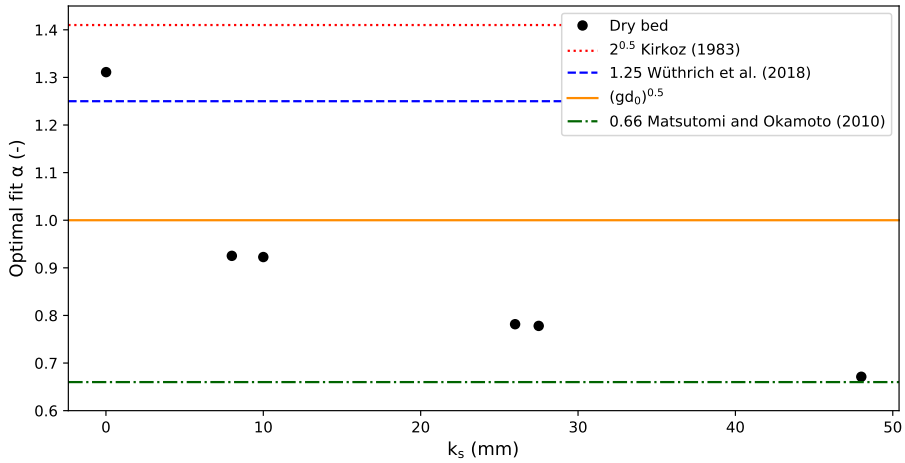

Figure 5.8: The influence of k_s on the optimal fitting α value for ensemble median wavefront celerities of dry bed tests at ADM6 (x = 6.0 m) with d_0 = 0.4 m compared to α values found in previous studies (Kirkoz, 1983; Matsutomi and Okamoto, 2010; Wüthrich et al., 2018)

5.3. Effect of Initially Still Water Level on Wavefront Celerity

The ensemble median wavefront celerities for increasing initially still water levels for all the roughness configurations are shown in Figure 5.9. The initially still water levels are normalised using the reservoir depth. Reference bed (smooth) data showed good agreement with the theoretical solution of Stoker (1957) (Eq. 1.7) and the empirical approximation of Stoker's (1957) theory by Montes (1998), presented by Chanson (2004b) (Eq. 1.11). It can be seen that increasing the initially still water level results in an asymptotic behaviour toward the value predicted by Stoker (1957). For the Reference (smooth bed), 50 mm wet bed test, the wavefront celerity is decreased with 26% compared to the Reference, dry bed wavefront celerity. The wavefront celerity of the R7 (k_s = 48 mm), 50 mm wet bed test is increased with 37% compared to the R7 (k_s = 48 mm) dry bed celerity. Therefore it suggests that bed roughness has a decreasing dominance on the celerity for increasing initially still water level. With certain bed roughness configurations, it can be noticed that an increase in initially still water level leads to an increase in wavefront speed, which means that the water layer works as a lubricant, confirming the findings by Nielsen et al. (2022).

It is interesting to notice the difference between the tests with an initially still water level below ($h_0 < h_r$) or above ($h_0 > h_r$) the top of the nails. For the shorter nail configurations with a length of 19 mm above the plate (R3 and R4), the tailwater level is already above the nail tops for the 25 mm wet bed tests and the asymptotic value is reached earlier. The results of 7.5 mm wet bed tests with nail tops clearly above the water surface show a lower wavefront celerity. For the longer nail configurations, with a length of 39 mm (R5, R6 and R7), the nails are only underwater for 50 mm wet bed tests and the asymptotic value of Stoker (1957) is reached later. For the dry bed and wet bed tests with tailwater below the top of the nails, the celerity is reduced by the rough beds.

The effect of the initially still water level on the wavefront celerity, normalised using the typical celerity $\sqrt{gd_0}$, can be compared to Stoker's theory (1957) and to previously performed dam-break wave tests by Nielsen et al. (2022) and Wüthrich et al. (2019), shown in Figure 5.10. It can be noticed that the smooth bed tests for both datasets are consistent with theory of Stoker (1957) and results showed a good agreement with previous studies conducted under similar flow conditions (Nielsen et al., 2022). Wavefront celerity decreases monotonically with increasing initially still water level for $0 < h_0/d_0 < 0.15$ for relatively smooth beds ($k_s/d_0 < 0.002$). Furthermore, the wavefront celerities of larger bed roughness's (R6 k_s = 27.5 mm and R7 k_s = 48 mm) are lower than the velocities measured by Nielsen et al. (2022) despite having a larger k_s value. Such difference in roughness values can be explained by the fact that these values are obtained using different measurement techniques, in line with previous findings by (Leng and Chanson, 2014).

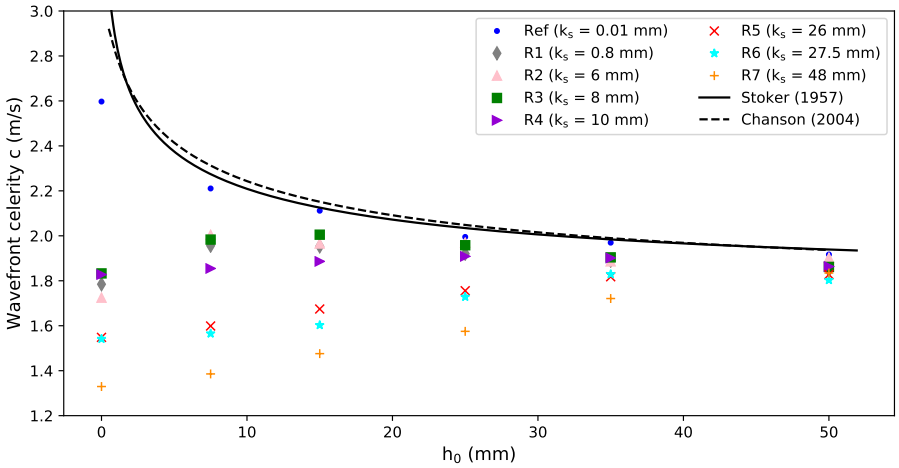

Figure 5.9: The effect of an initially still water level on the ensemble median wavefront celerity, for smooth and rough beds (d_0 = 0.4 m) compared to Stoker's (1957) theory (Eq. 1.7) and Montes' (1998) approximation (Eq. 1.11) for smooth, wet beds presented by Chanson (2004b)

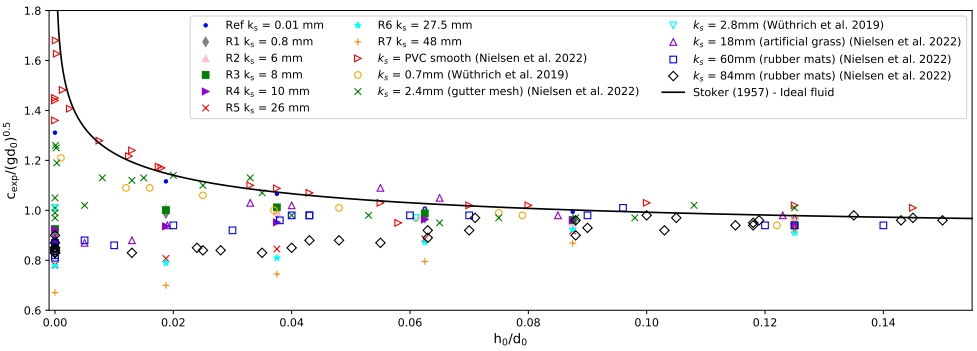

Figure 5.10: A comparison of ensemble median quasi-steady wavefront celerities, normalised using the typical celerity $\sqrt{gd_0}$, for increasing initially still water levels with data provided in Nielsen et al. (2022) and Stoker's (1957) theory for tests with a d_0 value of 0.4 m

A comparison of the wavefront celerities of this experimental work and previous data by Nielsen et al. (2022) including both bed roughness and the initially still water level is presented in Figure 5.11. The wavefront celerity is normalised using the ideal celerity predicted by the Stoker (1957) theory thorough the MacLaurin series (Eq. 1.8) developed by Nielsen et al. (2022). Data confirmed that the celerity converges to Stoker's model as the tailwater depth becomes greater than $0.5k_s$. The difference visible in Figure 5.11 in $k_{s;\text{present study}}/k_{s;\text{Nielsen (2022)}}$ of around 0.5 is in line with the differences in bed roughness values obtained with different measurement techniques (Leng and Chanson, 2014). The roughness values of the presently studied beds obtained with the backwater approach are therefore underestimated as shown by Leng and Chanson (2014), who showed a factor of 2 difference between the two techniques for the determination of the roughness coefficient for the same material.
When this underestimation of k_s with a factor 2 is taken into account, the data of tests from Nielsen et al. (2022) also using d_0 = 0.40 m, data of test from Wüthrich et al. (2019) using 0.40 m < d_0 < 0.82 m and results of the present study show the same trend of converging to Stoker's 1957 theory for $h_0 > 0.5\,k_s$ (Figure 5.11, where the factor 2 difference is not taken into account for the present study results).

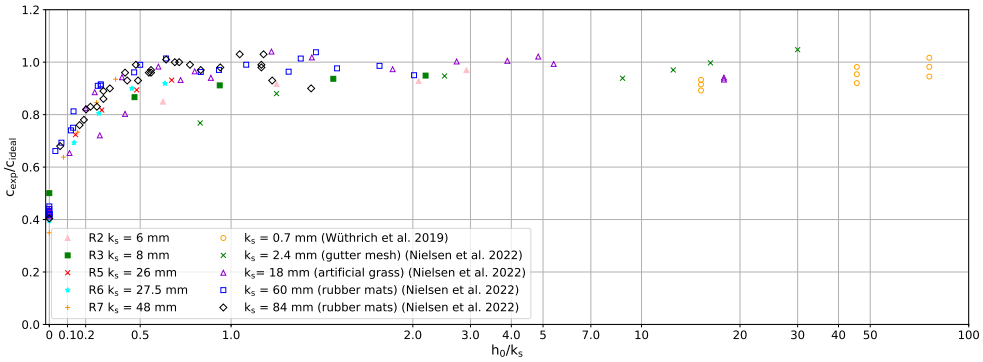

Figure 5.11: Quasi-steady wavefront celerities for dam-break waves (d_0 = 0.4 m) on rough beds ($1xk_s$) reaching Stoker's ideal celerity for $h_0/k_s > 0.5$, using Equation 1.8 for c_{ideal} compared with data of Nielsen et al. (2022)

A model to calculate the wavefront celerities with combinations of initially still water level and relatively small bed roughness was recently presented by Nielsen et al. (2022) and resulted in Equation 1.15. For the test configurations with small 'friction length' ($k_s/d_0 < 0.01$), where this equation is valid, the results of the present study are compared to the results of Nielsen's 2022 study in Figure 5.12. The experimental data of the present study is in good agreement with the experimental data and the model provided by Nielsen et al. (2022). The small resistance contributions h_0, $13k_s$ and $1700\nu/\sqrt{gd_0}$ have indeed similar effects on the wavefront celerity and they could act additively.

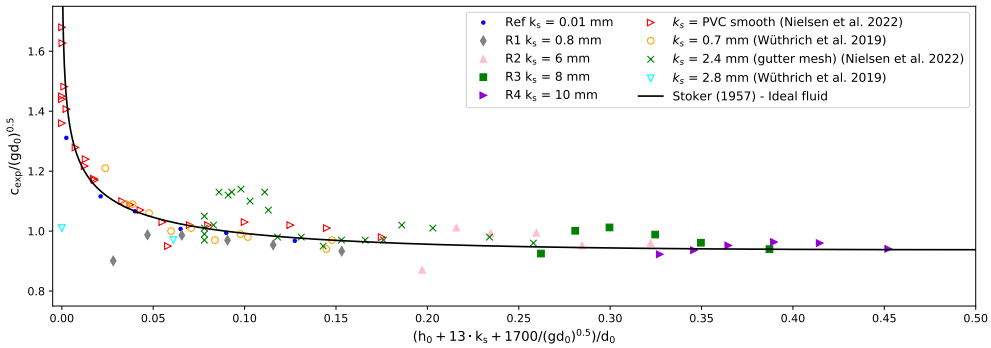

Figure 5.12: Combined effect of initially still water level, viscosity and bed roughness on the wavefront celerity calculated using Equation 1.15, normalised using the typical celerity $\sqrt{gd_0}$, compared to Stoker's (1957) theory and data provided in Nielsen et al. (2022)

5.4. Effect of Bed Roughness on Maximum Water Depth

If we specifically look at the influence of bed roughness on the maximum water depth (h_{max}), an increasing maximum water level is observed for increasing bed roughness in Figure 5.13, except for the wet bed 50 mm bores. The ensemble medians of all maximum water levels of the dry, 7.5, 15, 25, and 25 mm wet bed, R7 (k_s = 48 mm) configuration are increased by 12 to 43% compared to their Ref (smooth beds) configurations. The 50 mm wet bed R7 (k_s = 48 mm) configuration has a maximum water level of 85% of the dry bed, Ref (smooth) bed configuration.

Roughness configuration R3 (k_s = 8 mm) shows a lower maximum water level compared to the adjacent configurations R2 (k_s = 6 mm) and R4 (k_s = 10 mm). The maximum water depth for the Reference configuration (dry, smooth bed test) is around 0.135 m, which is 76% of the theoretical maximum water depth of 0.178 m based on the $4/9d_0$ condition of Ritter (1892) shown in Figure 1.5. Results of wet bed 35 and 50 mm tests with roughness configurations R3 (k_s = 8 mm) and R4 (k_s = 10 mm) appeared to be influenced by reflection of the wave at the downstream end of the flume and results were therefore not considered. The reflection waves were also visible during the tests and proved by the side view videos.

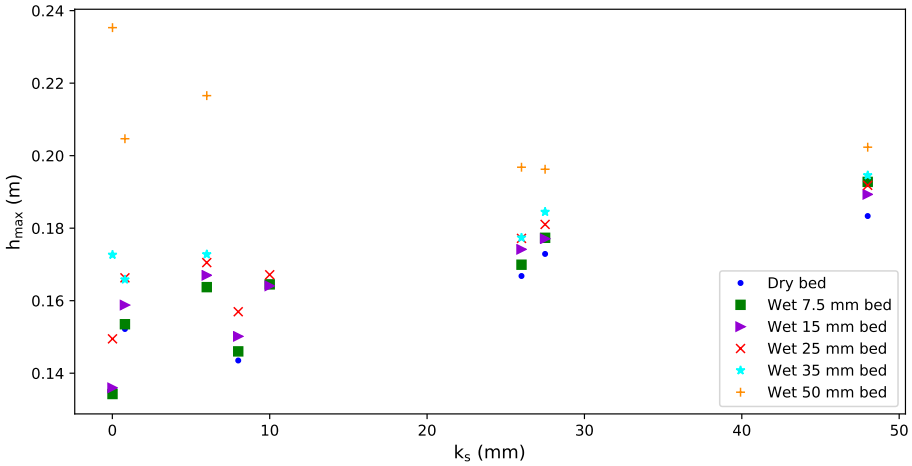

Figure 5.13: Experimental obtained maximum water depths (h_{max}) showing the influence of bed roughness (k_s) for tests with an initially water level in a range of 0 to 50 mm, d_0 = 0.4 m at ADM6 (x = 6.0 m)

5.5. Effect of Initially Still Water Level on Maximum Water Depth

Figure 5.14 shows the development of the maximum water depth for increasing initially still water levels. For the smaller still water levels (h_0 < 15 mm), the maximum wave height seems to be constant. For the larger still water levels (h_0 > 25 mm), the maximum water depth increases with increasing initially still water level in Figure 5.14, especially for low roughness configurations Ref (smooth), R1 (k_s = 0.8 mm) and R2 (k_s = 6 mm). The increase of h_{max} with increasing h_0 could be expected because of the constant discharge that is released over a downstream flume with an increasing existing water layer. Therefore, the effect of h_0 on $(h_{max} - h_0)/h_{max;dry\ bed}$ is shown in Figure 5.15. It shows that for the Reference (smooth) bed configuration an increase of h_0 leads first to a decrease of h_{max} for h_0 < 25 mm and an increase of h_{max} for h_0 > 35 mm. For larger roughness configurations (k_s > 8 mm) h_{max} seems to decrease with increasing h_0.

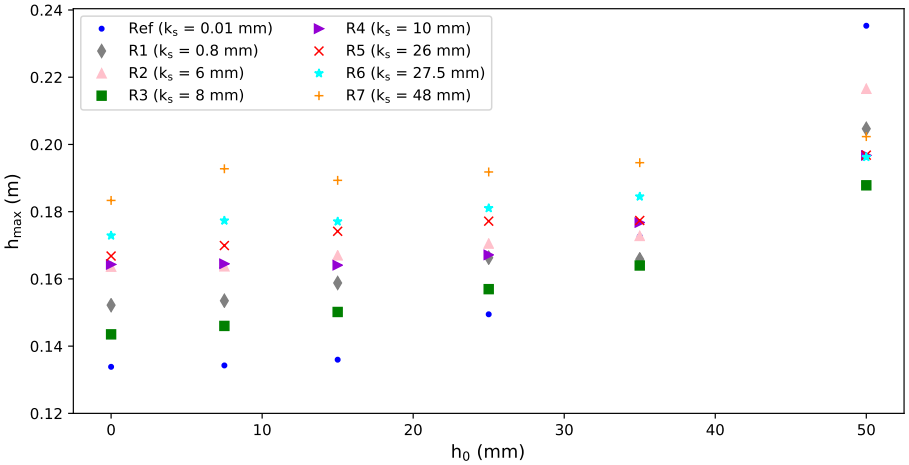

Figure 5.14: Experimental obtained maximum water depths (h_{max}) showing the influence of initially still water levels (h_0) for tests with a bed roughness (k_s) in a range of smooth to 48 mm, d_0 = 0.4 m at ADM6 (x = 6.0 m)

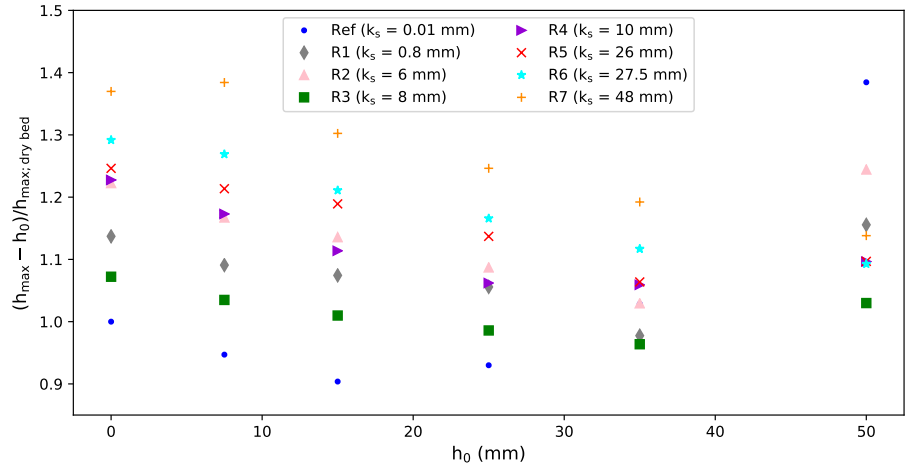

Figure 5.15: The effect of increasing initially still water level on the relative maximum water depth, normalised using the maximum water depth for dry bed tests at ADM6 (x = 6.0 m), for tests performed with d_0 = 0.4 m

A preliminary formula to calculate h_{max} for the combined effect of h_0 and k_s for h_0/d_0 < 0.0625 is presented in Appendix D. This empirical formula is not presented in the main report because the constants in the formula depend on the exact bed roughness values which must be researched more via a deeper analysis of the boundary.

5.6. Effect of Bed Roughness on Plateau Height

During the analysis, the plateau heights (h_2) appeared for only some configurations. The presence of plateau heights for combinations of roughness configurations and initially still water levels are shown in a contour plot (Figure 5.16). A clear, straight dividing line can be seen for this study. For dry bed tests, no plateau height was visible, which is in contrast with results obtained by Nielsen et al. (2022) for tests with small tailwater layers. In this Section, only tests that revealed the presence of a plateau height were investigated.

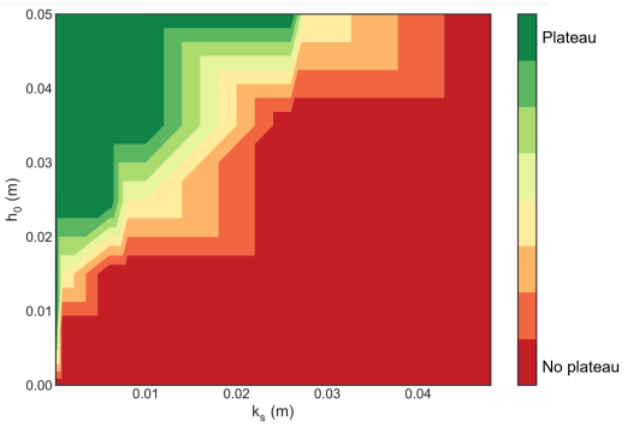

Figure 5.16: Contour plot showing the presence of a plateau height for dam-break wave tests with different combinations of h_0 and k_s with d_0= 0.4 m at ADM6 (x = 6.0 m)

The effect of bed roughness on the plateau height is shown in Figure 5.17 and it can be noticed that an increase in bed roughness seems to lead to an increase in plateau height for initially still water levels below 35 mm. The plateau heights for the wet bed 50 mm tests seem to show the opposite behaviour, including a decrease in plateau height with an increase in roughness. This shows some conflict with the existing theory and previously performed tests (Nielsen et al., 2022).
The plateau heights from this study are compared with the plateau heights based on the theory of Chanson et al. (2000), calculated with Equation 1.10. It can be noticed that almost all measured plateau heights are lower than the theoretical plateau heights, independent of k_s.

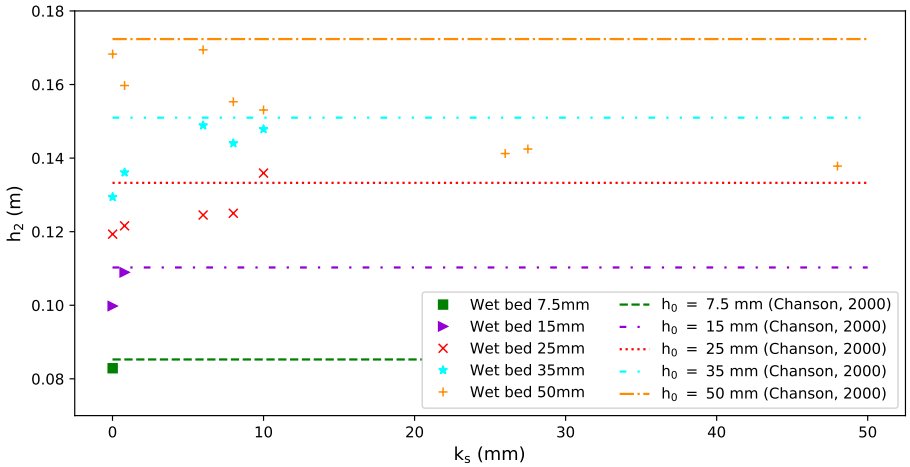

Figure 5.17: The effect of increasing bed roughness (k_s) on the plateau height for wet bed tests at ADM6 (x = 6.0 m) performed with d_0 = 0.4 m, in case a plateau height was observed, compared to the plateau heights based on theory of Chanson et al. (2000) (Eq. 1.10)

5.7. Effect of Initially Still Water Level on Plateau Height

The effect of an initially still water level on the plateau height of the dam-break waves is shown in Figure 5.18. The results of the reference configuration (smooth bed) show good agreement with Chanson et al. (2000) and the plateau heights of the rougher bed configurations show an increasing trend for increasing initial still water levels. Lower plateau heights are noted for $h_0/d_0 > 0.06$ tests compared to Chanson's (2000) theory, which is also observed with the data of Nielsen et al. (2022) in Figure 5.19. The initially still water level limit ($h_0/d_0 = 0.138$) presented by Stoker (1957) is respected in this study (Figure 5.18).

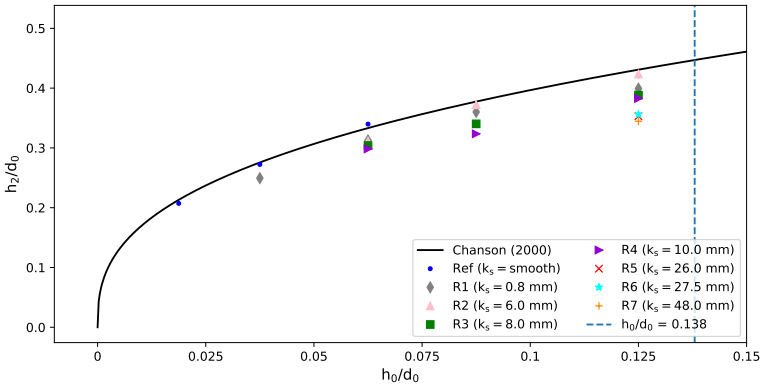

Figure 5.18: Influence of initially still water level on experimental obtained h_2 values respecting Stoker's (1957) limit $h_0/d_0 = 0.138$ and comparing to theory of Chanson et al. (2000)

The outcome of the present study is compared to data provided by Nielsen et al. (2022) (Figure 5.19). The graphs can be divided into 3 sections:

- The test results for values $h_0/d_0 < 0.06$ are showing some differences in behaviour. There were only plateaus observed for the small roughness configurations Ref (smooth) and R1 (k_s = 0.8 mm), which is in contrast with results of Nielsen et al. (2022) showing plateau heights with an asymptotic value around $h_2/d_0 = 0.35$ for rougher beds, higher than the theoretical solution. The plateau height of the Ref (smooth) and R1 (k_s = 0.8 mm) roughness configurations of present study follow the theory of Chanson et al. (2000). Results for smaller roughness configurations of Nielsen et al. (2022) followed the theory of Chanson et al. (2000) as well. Moreover, for the dry bed tests, no plateau height was visible in the present study, while is was the case for Nielsen et al. (2022).

- The second section in the graph, $0.06 < h_0/d_0 < 0.16$, shows good agreement between the present test results and the results of Nielsen et al. (2022), although the trend of a decreasing plateau height for increasing initial still water level is only seen for the present results. The absence of a plateau height for some configurations can be explained by the different roughness configurations used in the two studies. The plateau heights are lower than the smooth theoretical values obtained with Chanson's (2000) theory.

- Results for $h_0/d_0 > 0.16$, the third section are not obtained during this study because of respecting Stoker's (1957) limit. The results of Nielsen et al. (2022) show good agreement with the smooth theoretical values of Chanson et al. (2000), therefore roughness seems to have no influence on the plateau height for $h_0/d_0 > 0.16$.

A preliminary formula to calculate h_2 for the combined effect of h_0 and k_s is presented in Appendix E. This empirical formula is not presented in the main report because the constants in the formula depend on the exact bed roughness values which must be researched more via a deeper analysis of the boundary.

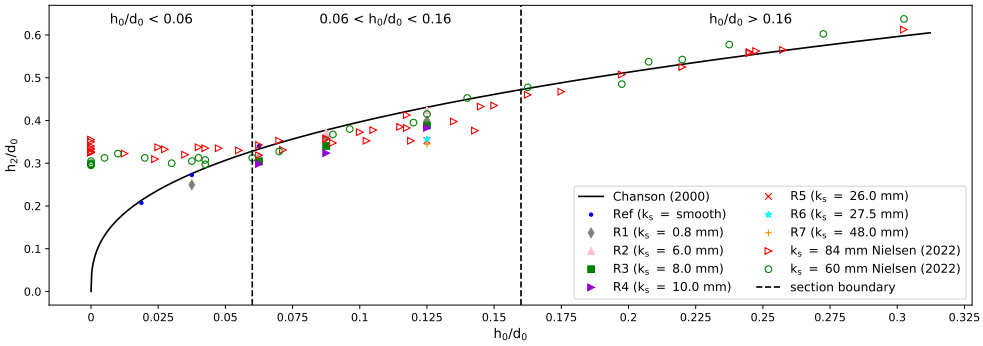

Figure 5.19: Comparison of h_2 values of present study at ADM6 (x = 6.0 m) and data provided by Nielsen et al. (2022) (both studies using d_0 = 0.4 m) with theory of Chanson et al. (2000)

5.8. Effect of Bed Roughness and Initially Still Water Level on Roller Length

With the wavefront celerities, presented in Sections 5.2 and 5.3, and the plateau heights, presented in Sections 5.6 and 5.7, the roller lengths (L_r) can be determined in case a plateau was present using the relation: $s = v \cdot t$ with s = horizontal distance from the wave tip, positive in upstream direction. The influences of the bed roughness and initially still water level on the roller length are shown in Figures 5.20 and 5.21. This preliminary investigation did now show a clear trend between k_s and the roller length for the bores. The wet bed 50 mm tests with plateau height for all roughness show a quite steady roller length. For an increasing tailwater the roller length seems to be quite constant, especially for the Reference (smooth) bed configuration. No clear trend in the data could be explained by the combined effects of k_s and h_0 on the plateau height. Overall, the determined roller lengths are relatively short compared to previous studies (Wüthrich et al., 2018).
The video analysis showed agreement with the water levels measured by ADM6 (x = 6.0 m) and the wavefront celerities measured between ADM5 and ADM6 (x = 5.0 & 6.0 m respectively), and so also agreement with reaching a certain water level after a certain duration of time after arrival of the wavefront. On the other hand, the wavefront seems to reach a calmer water level (plateau height) after at a later time, resulting in lengths between 0.2 to 0.3 m. This more turbulent constant water level can be seen in Figure 4.2.

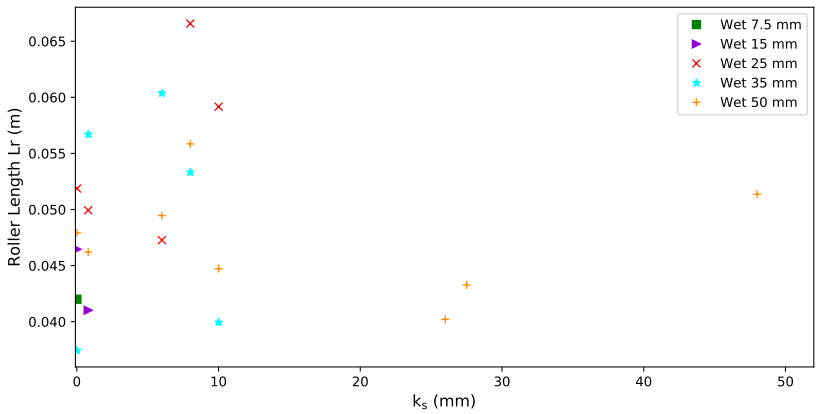

Figure 5.20: Experimental obtained roller lengths (L_r), in case a plateau height was observed, showing the effect of increasing bed roughness (k_s) on wet bed bores at ADM6 (x = 6.0 m) performed with d_0 = 0.4 m

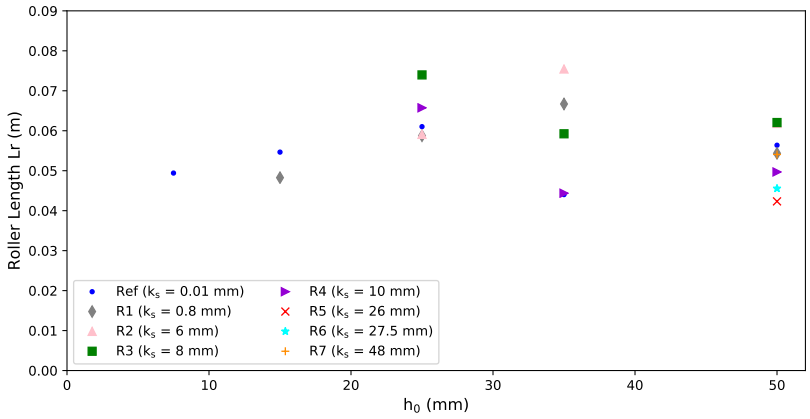

Figure 5.21: Effect of initially still water level on experimentally obtained roller lengths for wet bed tests with various bed roughnesses (d_0= 0.4 m)

The rise of water levels over the roller length is shown in Figure 5.22 combined with the results from previous studies by Chanson (2011); Wüthrich et al. (2018). The theory for -0.3 < $(x-x_s)/L_r$ < 0 underestimates the water depths compared to the self-similar profiles of the present study and where therefore left out in this analysis (black markers in Figure 5.22). The profiles for $(x-x_s)/L_r$ > -0.3 show better agreement with literature (colored markers in Figure 5.22). The best fitting N-value for Equation 1.16 for the present study is determined and presented in a contour plot (Figure 5.23). Most of the test configurations are consistent with the N-values from literature. For the test configurations with low bed roughness and small initial water levels, the best fitting N-value is higher compared to previous studies of Chanson (2011); Wüthrich et al. (2018).

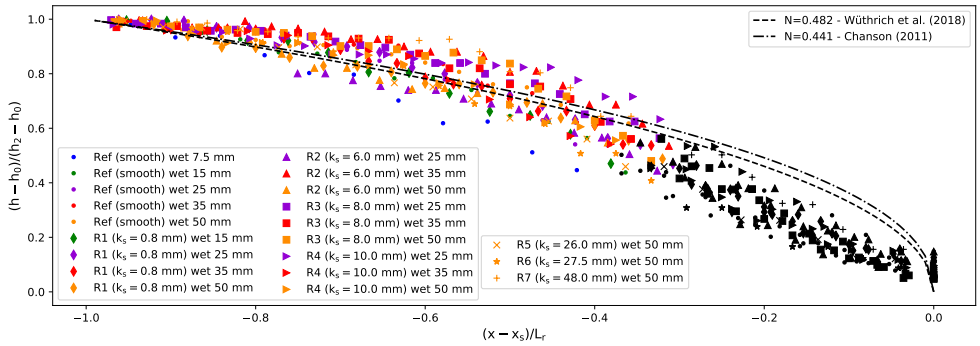

Figure 5.22: Comparison of the rise of the water level over the roller length of the present study (d_0= 0.4 m) to previous studies by Chanson (2011); Wang and Chanson (2013); Wüthrich et al. (2018)

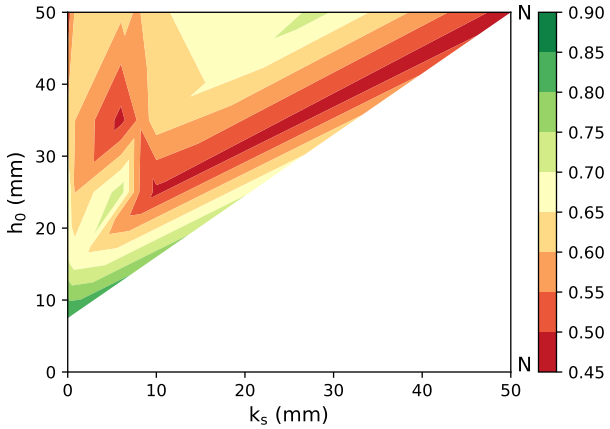

Figure 5.23: Contour plot showing the fitting N-value for the calculation of the roller length for dam-break wave tests with different combinations of h_0 and k_s with d_0= 0.4 m that showed the presence of a plateau height

6

Discussion

This Chapter describes the limitations and the uncertainties associated with this research project.

- There exist some uncertainties associated with the determination of the roughness values of the tested configurations. The backwater method used in this study and described in Appendix B leads to values that (likely) underestimate the roughness coefficients of both the natural and artificial created roughness beds. Hints are given by the fact that, the wavefront celerities for R7 (k_s = 48 mm) for $h_0/d_0 < 0.09$ are lower than the celerities for k_s = 84 mm by Nielsen et al. (2022) indicating that the roughness value of R7 (k_s = 48 mm) should be higher than the highest roughness (k_s = 84 mm) in the Nielsen (2022) study, using the analysis of the boundary layer to investigate the roughness coefficient. Moreover, Leng and Chanson (2014) showed a factor of 2 difference between the two techniques for the determination of the roughness coefficient for the same material. A more quantitative analysis can only be conducted once precise values of the bed roughness are determined. The estimation of the bed roughness should be done through a detailed analysis of the velocity profiles in boundary layer during the steady flow tests.
- This study showed some counter-intuitive results with missing plateaus heights for the different combinations of bed roughness and initially still water levels. This might be attributed to reflection of the dam-break wave in the downstream part of the channel or to the nature of the nails in reproducing roughness. The uniformity of the roughness of the beds created with nails might differ compared to gravel or rubber mats by Nielsen et al. (2022), therefore affecting the dam-break wave.
- The constriction of 5 mm on both side of the channel at the gate location was kept minimal and the effect of this constriction was reduced using wooden plates with contraction rate of 1:10, but this might have affected both wave propagation of the dam-break wave and the free-surface during the steady flow tests, hence increasing the uncertainty in the computation of the bed roughness.
- The ADMs measured the distance to an average surface. The arrival time of the wave was determined based on changing this measured distance from the ADMs to this surface. When a change in water level was detected, the wave only arrived at the most upstream boundary of the measurement surface, and not exactly right below the ADM location, as was assumed during this study. When measuring an interval time between two ADMs for determining the wavefront celerity, this effect plays a role for both ADMs and cancels each other out.
- The last general discussion point is that the results are obtained via experimental work and although great care was taken during the tests, however some minor inaccuracies could have affected the test results.

7

Conclusions and Recommendations

7.1. Conclusions

The impact of dam-break waves, storm surges and impulse waves propagating on land can be reduced through a better understanding of its hydrodynamic properties, including the effect of bed roughness. Currently, a link between bed roughness and hydrodynamic properties of dam-break waves is still missing. Hence, the effect of bottom roughness on the hydrodynamic properties of dam-break waves, on both dry and wet beds is the objective of this study, using an experimental approach. Dam-break waves were generated through a lift-gate and the water level over time was measured in the downstream channel. The parameters wavefront celerity, maximum water level, plateau height and roller length used to describe the hydrodynamic properties of the wave. Using gravel and nails, 7 different bed roughness configurations were reproduced with a range of $0.6 < k_s < 48$ mm in addition to the smooth bed reference test. Dry bed tests were performed at least 5 times per bed roughness, 5 wet bed tests with a range of $0 < h_0/d_0 < 0.125$ were performed at least 10 times per bed roughness.

Results for smooth and rough bed tests showed consistency with previous studies and theories. To generate a more detailed behaviour of the wave in the downstream channel, a new approach was used where water levels were extracted in a time zone just before and after the wavefront tip arrival. The dry, smooth bed water level results were consistent with Ritter's (1892) and Whitham's (1955) theory and the wet, smooth bed results were consistent with Whitham's (1955) and Stoker's (1957) theory. The rough bed results showed quasi-steady wavefront celerities, maximum water levels and plateau height, confirming that the wave is well developed at the location where data were acquired. The results of the dam-break waves generated with the facility of the present study were shown to be consistent with theory and literature.

Visual observations of the generated waves allowed for a better interpretation of the experimental results, through some simple image processing of side videos. In line with literature, a substantial difference in wavefront behaviour was observed between dry and wet bed tests. The dry bed surges showed a more constant rise in water level without any breaking. The wet bed bore had a more turbulent front characterized by strong aeration and a steeper bore fronts. The Reference dry bed showed no wave breaking, but higher bed roughness configurations seem to lead to a steepening of the wavefront resulting in wave breaking and therefore an increase in turbulence and air-entrainment in the wave.

The measured water depths over time showed different behaviours indicating that the wavefront celerity, maximum water level, plateau height and the roller length of the dam-break wave are affected by dry or wet and smooth or rough beds.

- The wavefront celerity of a dry bed test is highly influenced by the bed roughness and an increase in bed roughness leads to a decrease in celerity. Wet bed tests seemed to be less affected by bed roughness and it was shown that the initially still water level can actually work as a lubricant resulting in wavefront celerities with an asymptotic behaviour to the theoretical celerities by Stoker's (1957) theory, for tests with $h_0 > 0.5k_s$. These results confirm the findings in literature and show that the effect of an

initially still water level is dominant over bed roughness. Moreover, data showed good agreement with the model presented by Nielsen et al. (2022) combining the effects of bed roughness and initially still water levels for small friction lengths (h_0/d_0, k_s/d_0 and $\nu/\sqrt{gd_0^3}$).

- The maximum water level was also affected by both bed roughness and initially still water levels. For dry bed tests an increase in maximum water level was observed when increasing the bed roughness, which is the opposite for the maximum water levels for 50 mm wet bed tests. Increasing the initially still water level reduces the relative maximum water level for rough bed configurations. The Reference bed configuration shows an opposite behaviour, an increase of the maximum water level for an increase in initially still water level.

- In the present study, only some test configurations revealed the presence of a plateau height. If there was one, an increase in bed roughness showed a decrease in plateau height for bores with $h_0/d_0 = 0.125$. The results of the reference configuration (smooth bed) showed good agreement with the empirical expression presented by Chanson et al. (2000) while the plateau heights of rougher bed configurations show an increasing trend for increasing initial still water levels. For an increase in initial still water level, three behaviours were observed. The test results for values $h_0/d_0 < 0.06$ for smooth bed tests are in line with Chanson et al. (2000), but the results of Nielsen et al. (2022) show an asymptotic trend to $h_2/d_0 = 0.35$ higher than the theoretical solution. The results in the $0.06 < h_0/d_0 < 0.16$ section show good agreement between the present test results and the results of Nielsen et al. (2022), lower than the smooth theoretical values obtained with Chanson's (2000) theory. For $h_0/d_0 > 0.16$, results of Nielsen et al. (2022) show good agreement with the smooth theoretical values of Chanson et al. (2000), therefore roughness seems to have no influence on the plateau height.

- The roller lengths were determined with the wavefront celerity and the plateau height, in case one was present. No trivial relations were found for the influence of bed roughness or initial still water level on the roller length of the dam-break waves. The optimal fitting N-value for Equation 1.16 was determined resulting in N-values in a range of 0.48 to 0.85, which are in line with literature on breaking waves and hydraulic jumps.

Despite the effort made, only qualitative results were derived in the present study, mostly associated with the uncertainties linked with the determination of the roughness values. A full quantitative analysis can be conducted once precise values of the bed roughness configurations of the natural and artificial created roughens beds are determined. The backwater method used in this study leads to values that are likely underestimated the roughness coefficients, as detailed in the discussion.

Despite these limitations, these results provide some relevant contribution for a more detailed assessment of the role of roughness in the hydrodynamic behavior of dam-break waves.

7.2. Recommendations

- For a more precise determination of the instantaneous wavefront celerity a comparison between the ADM data and the side view videos could be further implemented. In this study, the celerity was determined on the basis of two frames, but the speed over the duration of the video can be further analyzed by using more frames.

- When analyzing the measured data, it appeared that there was a need for more data for the area with relatively low initially still water levels ($h_0/d_0 < 0.06$) compared to the reservoir depth. Since creating low tailwater levels is difficult, experiments with varying reservoir depths could be useful.

- A full quantitative analysis can be conducted once precise values of the bed roughness configurations of the natural and artificial created roughens beds are determined. The estimation of the present bed roughness coefficients should be done through a deeper analysis of the boundary during steady flow tests.

- The influence of the length and density of the nails on the artificially created bed roughnesses can be further investigated when tests are performed with more bed configurations. The present study, with h_r 19 or 39 mm, suggested that the influence of the nail length was larger than the nail density, however, because only two nail densities and two nail lengths were used, no definitive conclusion can be drawn.
- An oscillation in the water levels can be seen during the rising part of the dam-break wave. The dominant frequency can be analysed and maybe be related to bed roughness. Due to time constraints, this was not analysed extensively in this study, but visually, it seems that the dominant frequency increases as bed roughness increases for the rising part of the wave.
- To prevent the effect of the reflection wave in the measured water levels, the measurement locations should be placed further upstream, however still in the well-developed wave zone in the channel.

References

Aleixo, R., Soares-Frazão, S., and Zech, Y. (2019). Statistical analysis methods for transient flows–the dam-break case. *Journal of Hydraulic Research*, 57(5):688–701.

Baldock, T. E. (2018). " Bed shear stress, surface shape and velocity field near the tips of dam breaks, tsunami and wave runup" by Peter Nielsen. *Coastal Engineering*, 142:77–81.

Bryant, E. (2001). *Tsunami: The underrated hazard*. Cambridge University Press, New York, 1st ed edition.

Chanson, H. (2004a). *Environmental hydraulics for open channel flows*. Elsevier Science & Technology.

Chanson, H. (2004b). The Hydraulics of Open Channel Flow. An Introduction. pages 346–361. Elsevier, Burlington, 2nd edition.

Chanson, H. (2006a). Analytical solutions of laminar and turbulent dam break wave. In *River Flow*, pages 465–474.

Chanson, H. (2006b). Tsunami surges on dry coastal plains: Application of dam break wave equations. *Coastal engineering journal*, 48(04):355–370.

Chanson, H. (2011). Hydraulic jumps: turbulence and air bubble entrainment. *La Houille Blanche*, 97(3):5–16.

Chanson, H. (2019). Physical modelling of semi-circular channels and low velocity zones - application to pipe culverts and upstream fish passage at less-than-design flows. Technical report, The University of Queensland.

Chanson, H. (2020). Statistical analysis methods for transient flows–the dam-break case. *Journal of Hydraulic Research*, 58(6):1001–1004.

Chanson, H., Aoki, S., and Maruyama, M. (2000). Experimental Investigations of Wave Runup Downstream of Nappe Impact: Applications to Flood Wave Resulting from Dam Overtopping and Tsunami Wave Runup. *Coastal/Ocean Engineering Report, No. COE00-2, Dept. of Architecture and Civil Eng., Toyohashi University of Technology, Japan*.

Docherty, N. J. and Chanson, H. (2010). *Characterisation of unsteady turbulence in breaking tidal bores including the effects of bed roughness*. School of Civil Engineering, The University of Queensland.

Docherty, N. J. and Chanson, H. (2012). Physical Modeling of Unsteady Turbulence in Breaking Tidal Bores. *Journal of Hydraulic Engineering*, 138(5):412–419.

Dressler, R. F. (1952). Hydraulic Resistance Effect Upon the Dam-Break Functions. Technical Report 3.

Dute, H. (2008). De grote overstroming van 1926. *https://dute.home.xs4all.nl/overstroming%201926.htm*.

Escande, L., Nougaro, J., Castex, L., and Barthet, H. (1961). Influence de Quelques Paramètres sur une Onde de Crue Subite à l'Aval d'un Barrage. *La Houille Blanche*, (5):565–575.

Esteban, M., Roubos, J. J., Iimura, K., Salet, J. T., Hofland, B., Bricker, J., Ishii, H., Hamano, G., Takabatake, T., and Shibayama, T. (2020). Effect of bed roughness on tsunami bore propagation and overtopping. *Coastal Engineering*, 157.

Faure, J. and Nahas, N. (1961). Étude numérique et expérimentale d'intumescences à forte courbure du front. *Houille Blanche*, (5):576–587.

FEMA (2001). Coastal construction manual: Principles and practices of planning, siting, designing, constructing, and maintaining residential buildings in coastal regions. Technical report, FEMA 55, Washington, DC.

Heller, V. (2011). Scale effects in physical hydraulic engineering models. *Journal of Hydraulic Research*, 49(3):293–306.

Henderson, F. M. (1996). Open channel flow. pages 304–313. Macmillan.

Hooshyaripor, F., Tahershamsi, A., and Razi, S. (2017). Dam break flood wave under different reservoir's capacities and lengths. *Sadhana - Academy Proceedings in Engineering Sciences*, 42(9):1557–1569.

Humanity House (2017). Rampen & Conflicten: Indonesië. Tsunami, 2004. *https://humanityhouse.org/rampen-conflicten-indonesie-tsunami-2004/*.

Iizuka, H. and Matsutomi, H. (2000). Damage due to the flooding flow of tsunami. In *Proceedings of Coastal Engineering, JSCE*, volume 47, pages 381–385.

Khzeri, N. and Chanson, H. (2015). Turbulent velocity, sediment motion and particle trajectories under breaking tidal bores: simultaneous physical measurements. *Environmental Fluid Mechanics*, 15(3):633–650.

Kirkoz, M. (1983). Breaking and run-up of long waves, tsunamis: Their science and engineering. In *Proceedings of the 10th IUGG international tsunami symposium*. Terra Scientific Tokyo.

LaRocque, L. A., Imran, J., and Chaudhry, M. H. (2013). Experimental and Numerical Investigations of Two-Dimensional Dam-Break Flows. *Journal of Hydraulic Engineering*, 139(6):569–579.

Lauber, G. and Hager, W. H. (1998a). Experiments to dambreak wave: Horizontal channel. *Journal of Hydraulic Research*, 36(3):291–307.

Lauber, G. and Hager, W. H. (1998b). Experiments to dambreak wave: Sloping channel. *Journal of Hydraulic Research*, 36(5):761–773.

Leng, X. and Chanson, H. (2014). *Propagation of Negative Surges in Rivers and Estuaries: unsteady turbulent mixing and the effects of the bed roughness*. University of Queensland. School of Civil Engineering,.

Leng, X. and Chanson, H. (2015). Unsteady turbulence in expansion waves in rivers and estuaries: an experimental study. *Environmental Fluid Mechanics*, 15(5):905–922.

Leng, X. and Chanson, H. (2017). Upstream Propagation of Surges and Bores: Free-Surface Observations. *Coastal Engineering Journal*, 59(1):1750001–1750003.

Madsen, P. A., Fuhrman, D. R., and Schäffer, H. A. (2008). On the solitary wave paradigm for tsunamis. *Journal of Geophysical Research: Oceans*, 113(C12).

Matsutomi, H. and Okamoto, K. (2010). Inundation flow velocity of tsunami on land. *Island Arc*, 19(3):443–457.

Meerssen (2021). Dijkdoorbraak in Limburgse Meerssen, oproep om zo snel mogelijk weg te gaan.

Montes, S. (1998). *Hydraulics of Open Channel Flow*. Amsterdam University Press, Amsterdam, Nederland.

Murty, T. S. (1977). *Seismic sea waves: tsunamis*. Ottawa, Ont.(Canada) Dept. of Fisheries and the Environment, Fisheries and Marine Services.

Nielsen, P. (2018). Bed shear stress, surface shape and velocity field near the tips of dam-breaks, tsunami and wave runup. *Coastal Engineering*, 138:126–131.

Nielsen, P. (2019). Bed shear stress, surface shape and velocity field near the tips of dam-breaks, tsunami and wave runup: Reply by Peter Nielsen. *Coastal Engineering*, 152:103513.

Nielsen, P., Xu, B., Wüthrich, D., and Zhang, S. (2022). Friction effects on quasi-steady dam-break wave propagation on horizontal beds. *Journal of Fluid Mechanics*, 939.

Rafferty, J. P. (2011). Japan earthquake and tsunami of 2011 | Facts & Death Toll.

Rafferty, J. P. and Pletcher, K. (2011). Japan earthquake and tsunami of 2011 | Facts & Death Toll.

Reichstetter, M. and Chanson, H. (2013). Unsteady turbulent properties in negative waves in open channels. *European Journal of Mechanics, B/Fluids*, 37:1–9.

Rijkswaterstaat (2021). Doorbraak Den Dommel februari 1953 ID320079. *https://beeldbank.rws.nl/MediaObject/Details/320079*.

Ritter, A. (1892). Die fortpflanzung der wasserwellen. *Zeitschrift des Vereines Deutscher Ingenieure*, 36(33):947–954.

Schoklitsch, A. (1917). Uber dammbruchwellen. *Sitzungberichten der Konigliche Akademie der Wissenschaften, Vienna, 126*, (1489-1514).

Shafiei, S., Melville, B. W., and Shamseldin, A. Y. (2016). Experimental investigation of tsunami bore impact force and pressure on a square prism. *Coastal Engineering*, 110:1–16.

Stoker, J. J. (1957). Water waves: The mathematical theory with applications. pages 308–341. Interscience Publishers, New York.

Stolle, J., Ghodoosipour, B., Derschum, C., Nistor, I., Petriu, E., and Goseberg, N. (2019). Swing gate generated dam-break waves. *Journal of Hydraulic Research*, 57(5):675–687.

Stolle, J., Goseberg, N., Nistor, I., and Petriu, E. (2018). Probabilistic Investigation and Risk Assessment of Debris Transport in Extreme Hydrodynamic Conditions. *Journal of Waterway, Port, Coastal, and Ocean Engineering*, 144(1):4017039.

Von Häfen, H., Goseberg, N., Stolle, J., and Nistor, I. (2019). Gate-Opening Criteria for Generating Dam-Break Waves. *Journal of Hydraulic Engineering*, 145(3):04019002.

Wang, H. and Chanson, H. (2013). Air entrainment and turbulent fluctuations in hydraulic jumps. *Urban Water Journal*, 12(6):502–518.

Watersnoodmuseum (2018). De Watersnoodramp. *https://watersnoodmuseum.nl/kennisbank/de-watersnoodramp/?gclid=CjwKCAiA1JGRBhBSEiwAxXblwTAVtzvrHd7EfuKXs8fuU4Tdej2ILBBYtH45C-geP656HXYlAr7AIRoCQdsQAvD_BwE*.

Whitham, G. B. (1955). The effects of hydraulic resistance in the dam-break problem. *Proceedings of the Royal Society of London. Series A. Mathematical and Physical Sciences*, 227(1170):399–407.

Wüthrich, D., Nistor, I., Pfister, M., and Schleiss, A. J. (2015). Experimental Generation of Tsunami-Like Waves. In *Coastal Structures and Solutions to Coastal Disasters 2015: Tsunamis - Proceedings of the Coastal Structures and Solutions to Coastal Disasters Joint Conference 2015*, pages 219–226.

Wüthrich, D., Pfister, M., Manso, P., Constantinescu, G., and Schleiss, A. (2016). Surface turbulence on bores and surges propagating on smooth and rough beds. In *Proceedings of the 6th International Conference on the Application of Physical Modelling in Coastal and Port Engineering and Science (Coastlab16)*.

Wüthrich, D., Pfister, M., Nistor, I., and Schleiss, A. J. (2018). Experimental Study of Tsunami-Like Waves Generated with a Vertical Release Technique on Dry and Wet Beds. *Journal of Waterway, Port, Coastal, and Ocean Engineering*, 144(4):04018006.

Wüthrich, D., Pfister, M., and Schleiss, A. J. (2019). Effect of bed roughness on tsunami-like waves and induced loads on buildings. *Coastal Engineering*, 152.

Wüthrich, D., Shi, R., and Chanson, H. (2020). Physical study of the 3-dimensional characteristics and free-surface properties of a breaking roller in bores and surges. *Experimental Thermal and Fluid Science*, 112.

Wüthrich, D., Shi, R., and Chanson, H. (2021). Strong free-surface turbulence in breaking bores: a physical study on the free-surface dynamics and air–water interfacial features. *Journal of Fluid Mechanics*, 924.

Xu, B., Zhang, S., Nielsen, P., and Wüthrich, D. (2021). Measurements of bed shear stresses near the tip of dam-break waves on a rough bed. *Experiments in Fluids*, 62(3).

A

Photos Roughness Configurations

This Appendix shows extra pictures of the roughness beds used for the dam-break wave tests.

Roughness 0
Smooth
k_s = 0.01 mm

Roughness 1
Small gravel
k_s = 0.8 mm

Roughness 2
Large gravel
k_s = 6.0 mm

Roughness 3
Small nails, low density
k_s = 8.0 mm

Roughness 4
Small nails, high density
k_s = 10.0 mm

Roughness 5
Long nails, low density
k_s = 26.0 mm

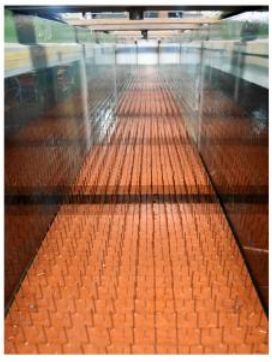

Roughness 6
Small and long nails, high density
k_s = 27.5 mm

Roughness 7
Large nails, high density
k_s = 48.0 mm

Figure A.1: Overview of roughness configurations seen from downstream end of the flume.

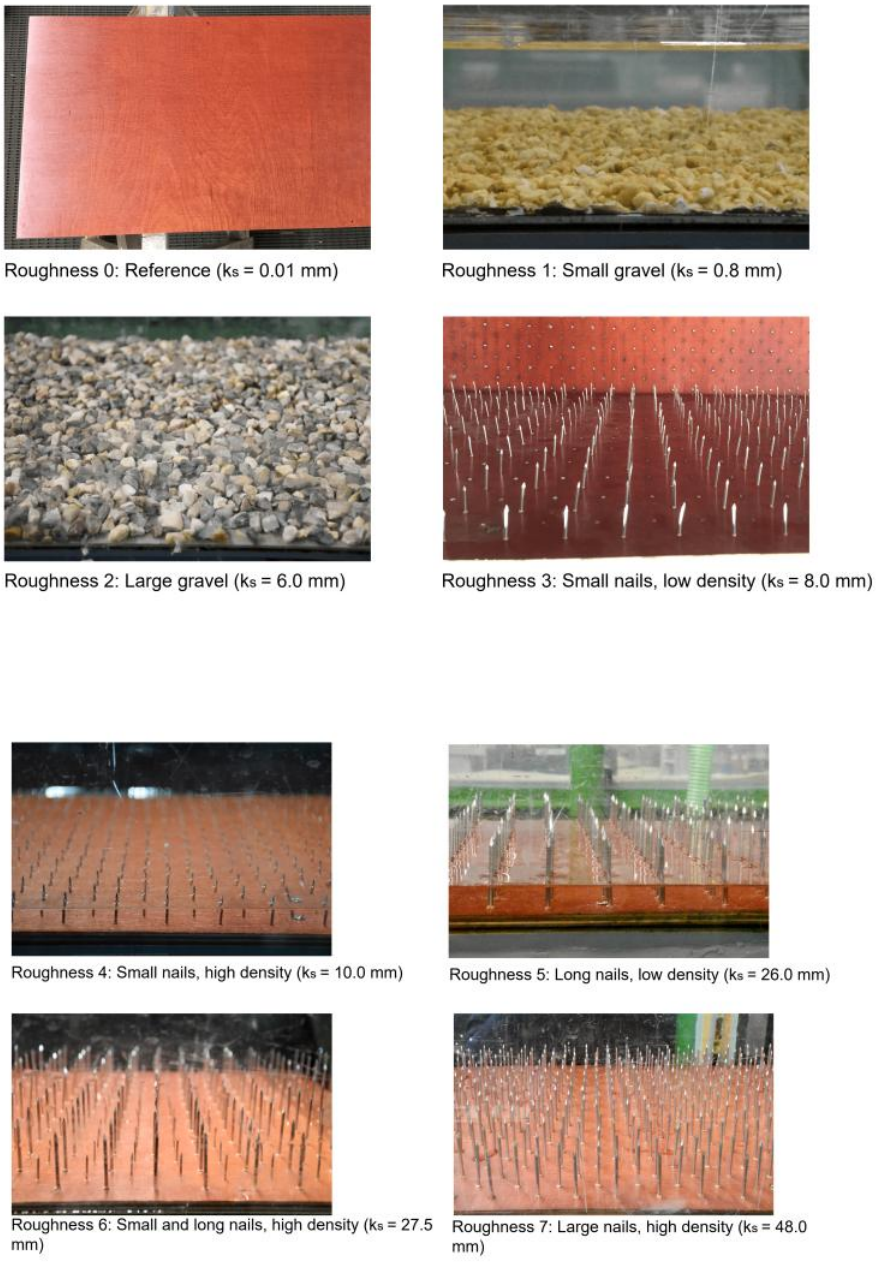

Figure A.2: Overview of details of roughness configurations seen from the top (Ref configuration) or side (other configuration)

B

Steady Flow Test

B.1. Set-up Steady Flow Test

To determine the bed roughness values, steady flow tests were performed in the 1st tilting flume (West) in the Hydraulic Engineering Laboratory at the TU Delft (Figure 2.1). The flume has a length of 14.3 m, a width of 0.40 m and a height of 0.42 m (Figures B.1 and B.2). In this test, several constant discharges were used ranging from 0.016 to 0.046 m^3/s. The data was collected with the following measurement equipment.

- The discharge was determined using a Rehbock weir. For this purpose, in the return flow of the flume, the **water level across the spillway in the return flume** was measured at a distance equal to twice the weir height. A rod style position sensor with an open ring magnet (Temposonics® GHM0300MD601A0, Cary USA) was used here. The measurement accuracy was ± 0.1 mm. This output value was given in Volts. By means of calibration with different discharges and manual measurements of the water levels in the return flow, the discharge was determined.
- The water levels were measured with a **point gauge** every 0.5 m from the gate to the downstream end of the flume (Figure B.1), with an accuracy of ± 0.5 mm.

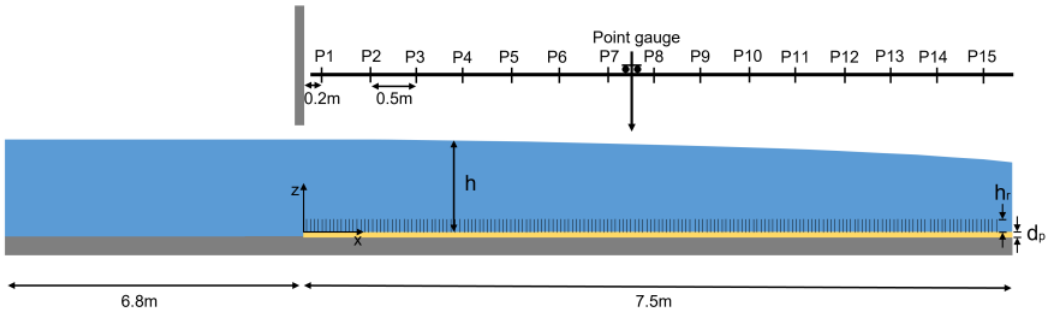

Figure B.1: Definition sketch of the steady flow set-up

For each roughness configuration, the water levels were measured for four different discharges. Discharges in the range of 0.006 to 0.030 m^3/s (see Table B.1) are commonly observed in literature (Leng and Chanson, 2014). Here, measurements were made with flow rates up to 40 l/s, above which the flow became unstable.

B.2. Obtaining Roughness Values

To calculate the friction factor in experiments, the friction slope of steady flow tests with the different bed roughnesses can be used (Chanson, 2004b, 2019). By reconstructing a backwater equation through the measured water levels, the friction factor can be determined (Leng and Chanson, 2014; Wüthrich et al., 2018).

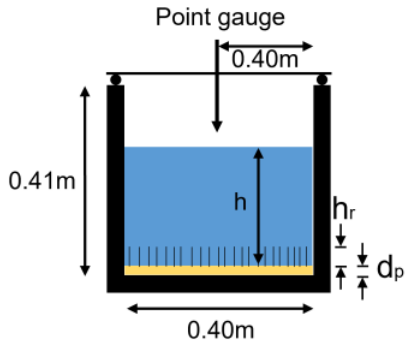

Figure B.2: Definition sketch of the steady flow set-up (crosssection)

Configuration	Discharge [Q (l/s)]	Flow velocity [U (m/s)]	Used point gauge numbers
Ref	7.10 to 18.07	4.43 to 5.37	1 to 15
R1	26.72 to 38.22	5.92 to 6.65	2 to 13
R2	23.89 to 39.65	5.78 to 6.74	2 to 13
R3	20.81 to 36.35	5.51 to 6.53	1 to 15
R4	12.37 to 42.38	4.50 to 5.90	1 to 15
R5	27.63 to 38.27	6.02 to 6.65	1 to 15
R6	29.00 to 41.15	6.10 to 6.80	1 to 15
R7	26.31 to 35.89	5.90 to 6.48	1 to 15

Table B.1: Experimental program and characteristics of the performed steady flow tests

In reconstructing the backwater curves, only the water levels measured above the roughness beds and not affected by the beginning and end of the row of plates were included. This was particularly important for the naturally created roughness values because these plates did not cover the entire downstream flume length.

To reconstruct the backwater curve, the following three formulas are used:

$$S_f = \frac{f \cdot Q^2 \cdot (W + 2h)}{8 \cdot g \cdot A^3} \tag{B.1}$$

$$f_{Colebrook-White} = \frac{1}{\left[-2 \cdot \log\left(\frac{k_s}{3.71 \cdot (\frac{W \cdot h}{W+2h})} + \frac{2.51}{Re\sqrt{f_{Altsul}}}\right)\right]^2} \tag{B.2}$$

$$f_{Altsul} = 0.1 \cdot \left(1.46 \cdot \frac{k_s}{\frac{W \cdot h}{W+2h}} + \frac{100}{Re}\right)^{1/4} \tag{B.3}$$

For each steady flow test an upstream and downstream backwater curve is reconstructed and compared to each other. Reconstructing a backwater curve is done by changing the input parameter k_s and check whether an optimal fit if found with the measured water levels over the downstream flume length. This k_s value is put in the Colebrook-White equation (Equation B.1) and the friction factor (f) is calculated. The formula is implicit, so to come up with a start value of f, the Altsul equation (Equation B.3) is used. This formula is explicit and therefore practical to generate a start value for the iterative process that will follow to find the friction factor with the Colebrook-White formula.
The reconstructed backwater curve is visually checked with the measured water levels (Figure B.3). This Figure shows the result of the downstream reconstructed backwater curve for the steady flow test of roughness configuration R2 (large gravel, k_s = 6.0 mm) with a discharge of almost 40 l/s. For this configuration the backwater curve is reconstructed for only point gauge numbers 2 to 13 while the roughness bed is not covering the whole downstream part of the flume and the last point gauges are effected by the outflow of the water at the end of the flume.

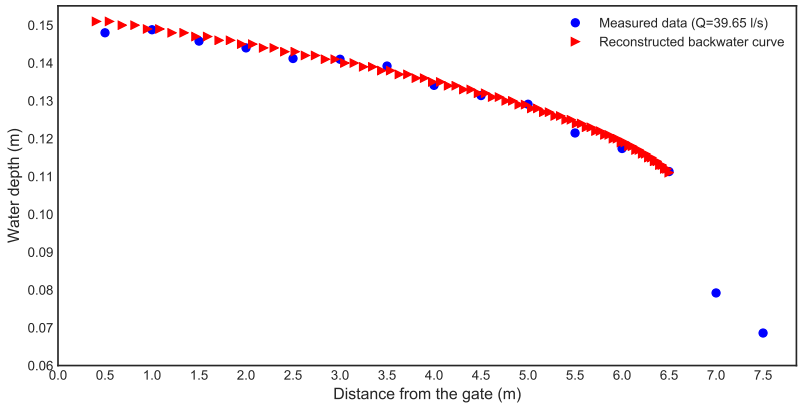

Figure B.3: Measured water levels and downstream reconstructed backwater curve (for point gauge numbers 2 to 13) for the steady flow test of roughness configuration R2 (large gravel, k_s = 6.0 mm) with a discharge of almost 40 l/s

During the determination of the bed roughness values no division was made between wall friction and bed friction.

B.3. Results Steady Flow Tests

The results of the steady flow tests are presented in Table B.2. It seems that extending the nails has a larger effect on soil roughness than increasing the density in the grid because the increase in roughness values between small nail configurations (R3 k_s = 8.0 mm and R4 k_s = 10.0 mm) and long nail configurations (R5 k_s = 26.0 mm, R6 k_s = 27.5 mm and R7 k_s = 48.0 mm) is large. Moreover, the difference between R5 k_s = 26.5 mm and R6 k_s = 27.5 mm (same as R5 k_s = 26.0 mm, small nails added to have high density grid instead) is very small.

Roughness name	**Abbreviation**	**Configuration**	k_s **(mm)**
Reference	Ref	smooth	0.01
Roughness 1	R1	small gravel (d_{50} = 2 mm)	0.8
Roughness 2	R2	large gravel (d_{50} = 5 mm)	6.0
Roughness 3	R3	19 mm nails, low density	8.0
Roughness 4	R4	19 mm nails, high density	10.0
Roughness 5	R5	39 mm nails, low density	26.0
Roughness 6	R6	19 mm and 39 mm nails, high density	27.5
Roughness 7	R7	39 mm nails, high density	48.0

Table B.2: Equivalent roughness values obtained reconstructing the backwater curves for the different roughness configurations through the measured water levels during steady flow tests

A bed roughness of 0.8 mm for small gravel is not physically possible, when compared to roughness configurations of previous performed tests (Nielsen et al., 2022). A difference in roughness values of $k_{s;\text{present study}}/k_{s;\text{Nielsen (2022)}}$ = 0.5 is in line with the differences in bed roughness values obtained using different measurement techniques (Leng and Chanson, 2014). The roughness values of the present studied beds obtained with the backwater curve method are therefore underestimated as shown by Leng and Chanson (2014). More research in obtaining the roughness values of naturally and artificially created roughness beds is highly recommended.

C

Comparison of Wavefront Celerity Data

This Appendix presents the wavefront celerities determined with the ADMs (between ADM5 and ADM6) and with the videos (through the glass sidewall around the location of ADM6). For some types of tests, no videos were made or the wavefront celerity cannot be calculated using the recorded material, see Table C.1 below. The difference in wavefront celerity can be explained by the difference in measurement method. The celerities obtained from video material have a larger margin of error due to the number of frames that can be made per second.

Wavefront Celerity [m/s]	**Configuration**	**Dry**	**7.5 mm**	**15 mm**	**25 mm**	**35 mm**	**50 mm**
VIDEO	Ref	-	-	-	-	-	-
ADM5-6	Ref	2.439	2.232	2.066	2.016	1.908	2.024
Difference ratio	Ref	-	-	-	-	-	-
VIDEO	R1	1.558	1.644	1.614	1.664	1.583	1.675
ADM5-6	R1	1.820	1.929	1.880	1.918	1.835	1.967
Difference ratio	R1	0.144	0.148	0.141	0.132	0.137	0.148
VIDEO	R2	1.535	1.679	-	1.764	1.779	1.730
ADM5-6	R2	1.692	1.951	1.938	1.942	1.923	2.024
Difference ratio	R2	0.093	0.139	-	0.091	0.075	0.145
VIDEO	R3	1.879	1.740	1.698	1.764	1.702	1.726
ADM5-6	R3	1.998	1.959	1.951	1.988	1.852	1.976
Difference ratio	R3	0.060	0.112	0.130	0.113	0.081	0.127
VIDEO	R4	-	-	1.670	1.700	1.730	-
ADM5-6	R4	1.786	1.786	1.821	1.845	1.797	1.890
Difference ratio	R4	-	-	0.083	0.079	0.037	-
VIDEO	R5	1.327	1.357	1.362	1.487	1.553	1.640
ADM5-6	R5	1.486	1.567	1.598	1.685	1.775	1.799
Difference ratio	R5	0.107	0.134	0.148	0.118	0.125	0.088
VIDEO	R6	1.467	1.295	1.377	1.468	1.623	1.562
ADM5-6	R6	1.523	1.506	1.565	1.727	1.792	1.835
Difference ratio	R6	0.037	0.140	0.120	0.150	0.095	0.149
VIDEO	R7	1.254	1.203	1.274	1.313	1.443	1.713
ADM5-6	R7	1.276	1.383	1.455	1.523	1.691	1.761
Difference ratio	R7	0.017	0.130	0.124	0.138	0.147	0.027

Table C.1: Comparison of wavefront celerities (in m/s) measured between ADM5 and ADM6 and calculated with the side view videos at ADM6 location

D

Preliminary Formula Maximum Water Depth

The experimental results of the maximum water depth of the present study are shown in Figure D.1. As was stated in Sections 5.4 and 5.5, there is a trend visible in the graph. Because the configurations with a relative large initially still water level are effected by a reflection wave, only the data of $h_0 < 25$ mm are analysed.

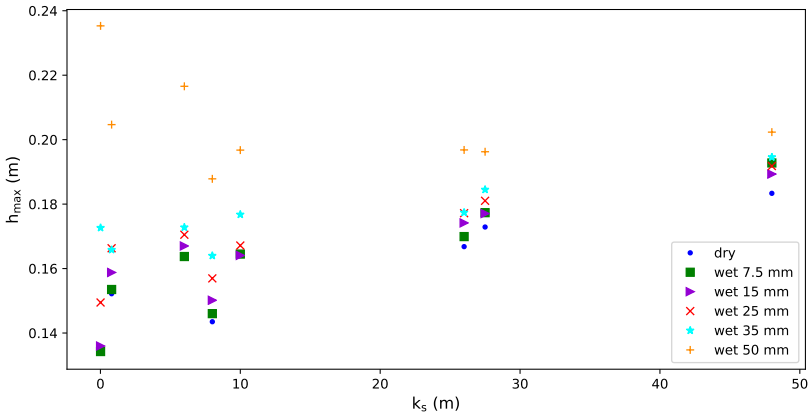

Figure D.1: Experimental obtained maximum water depths (h_{max}) showing the influence of initially still water levels (h_0) for tests with a bed roughness (k_s) in a range of smooth to 48 mm, d_0 = 0.4 m at ADM6

Because the trend seems to be linearly and the preliminary formula is kept as simple as possible, an optimal fit for the maximum water levels is found with the following formula:

$$\frac{h_{max} - h_0}{d_0} = C_1 \cdot \frac{k_s}{d_0} + C_2 \tag{D.1}$$

Because the formula must be useful for other test conditions (other d_0 values f.e.) as well, the parameters in the formula are normalised by the reservoir depth. The optimal fit resulted in an optimal value for C_1 and C_2 per still water level. The C_1 value changes with roughness, the change in C_2 was negligible. C_1 shows a decreasing trend when the initially still water level is increased. The outcome resulted in the following formula:

$$\frac{h_{max} - h_0}{d_0} = \left(-6.43\frac{h_0}{d_0} + 1.1\right) \cdot \frac{k_s}{d_0} + 0.35 \tag{D.2}$$

The outcome of Equation D.2 (h_{max} values) for several roughness values for tests with d_0 = 0.4 m can be seen in Figure D.2. Figure D.3 shows a comparison between the experimental obtained h_{max} and the h_{max} that

is calculated with Equation D.2. The coefficient of determination (R^2) between all experimental maximum water depths and calculated maximum water depths is 0.79.

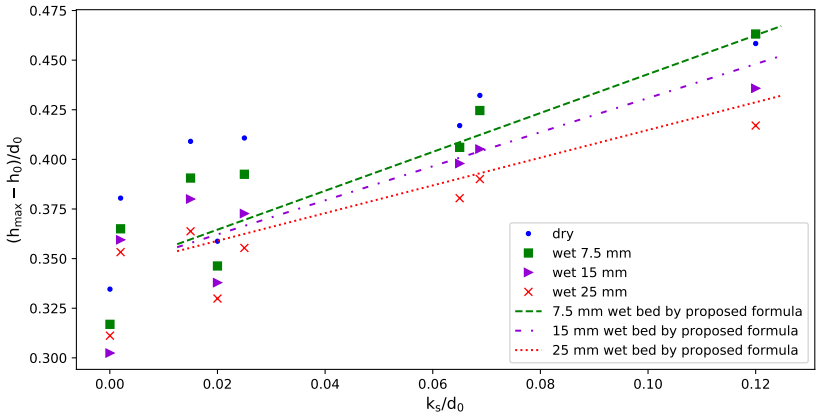

Figure D.2: Comparison of experimental obtained h_{max} (h_0= 0, 7.5, 15 and 25 mm tests with d_0= 0.4 m) and calculated h_{max} values with Equation D.2 for increasing roughness in a range from smooth to k_s = 48 mm

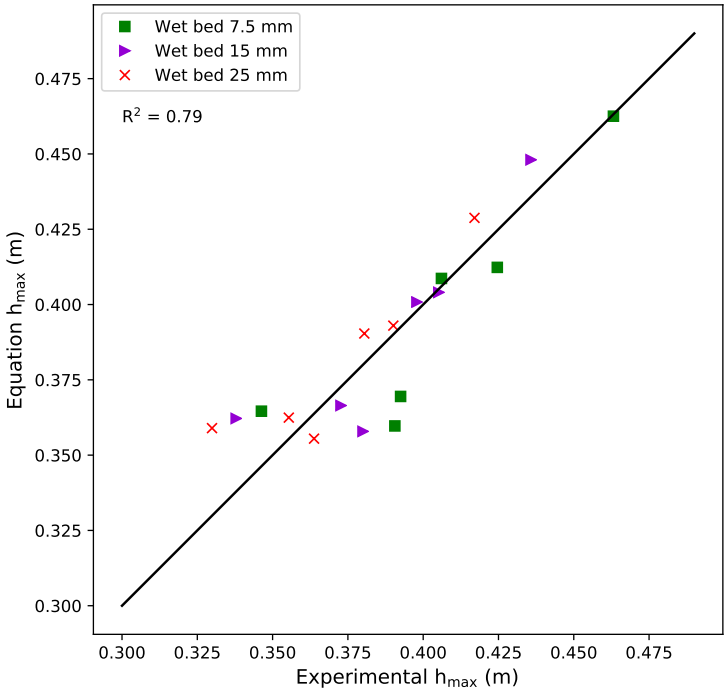

Figure D.3: Comparison of experimental obtained h_{max} (h_0= 7.5, 15 and 25 mm tests with d_0= 0.4 m) and calculated h_{max} values with Equation D.2

The presented empirical formula is not stated in the main report because the constants in the formula depend on the exact bed roughness values which must be researched more via a deeper analysis of the boundary. The approach used here to come up with the adapted formulas can be used when more accurate roughness values are obtained.

E

Preliminary Formula Plateau Height

The plateau height (h_2) is an important parameter to calculate the wavefront celerity of the dam-break wave. Chanson et al. (2000) came up with a formula (Equation 1.10) to calculate the plateau height taken into account the reservoir depth (d_0) and the initially still water layer (h_0). The outcome of Equation 1.10 can be used as input for Equation 1.6 to calculate the wavefront celerity, derived by Stoker (1957). Both formulas do not take into account the bed roughness. Of all parameters in Equations 1.6 and 1.10, only the plateau height changes when the bed roughness is changed, presented in Section 5.6. The experimental results of the plateau height of the present study are shown in Figure E.1. Although the results show some conflict with the existing theory and previously performed tests (Nielsen et al., 2022), a trend can be seen in the present study. In this Appendix, a preliminary relation between h_2, k_s and h_2 is presented.

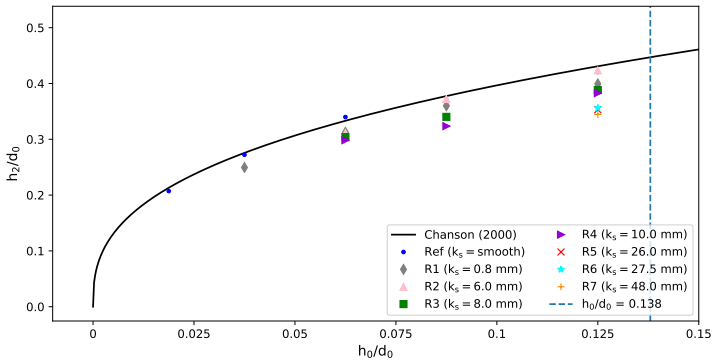

Figure E.1: Effect of initially still water level on plateau height for several roughness configurations, respecting the limit $h_0/d_0 = 0.138$ imposed by Stoker (1957) and comparing to theory of Chanson et al. (2000), Equation 1.10

In order to find a trend, only the roughness configurations where at least three plateau heights were found per bed roughness were analysed. An optimal fit by the data points of roughnesses Ref (smooth), R1 (k_s = 0.8 mm), R2 (k_s = 6 mm), R3 (k_s = 8 mm) and R4 (k_s = 10 mm)has been searched with the following function:

$$h_2 = d_0 \cdot C_1 \cdot \frac{h_0}{d_0}^{C_2} \tag{E.1}$$

The above equation was based on the formula presented by Chanson et al. (2000) because the trend of the plateau height behaviour for increasing initial still water levels seems to be the seem. The optimal fit resulted in an optimal value for C_1 and C_2 per bed roughness. The C_1 value changes with roughness, the C_2 was almost the same for each roughness configuration. C_1 shows a decreasing trend when the roughness is increased. Because the formula must be useful for other test conditions (other d_0 values f.e.) as well, the influence in roughness is normalised by the reservoir depth. The h_0 in Chanson's formula (Equation 1.10) is also normalised by d_0. The outcome resulted in the following formula:

$$h_2 = d_0 \cdot \left(-5.16 \cdot \frac{k_s}{d_0} + 1.64\right) \cdot \frac{h_0}{d_0}^{0.38} \tag{E.2}$$

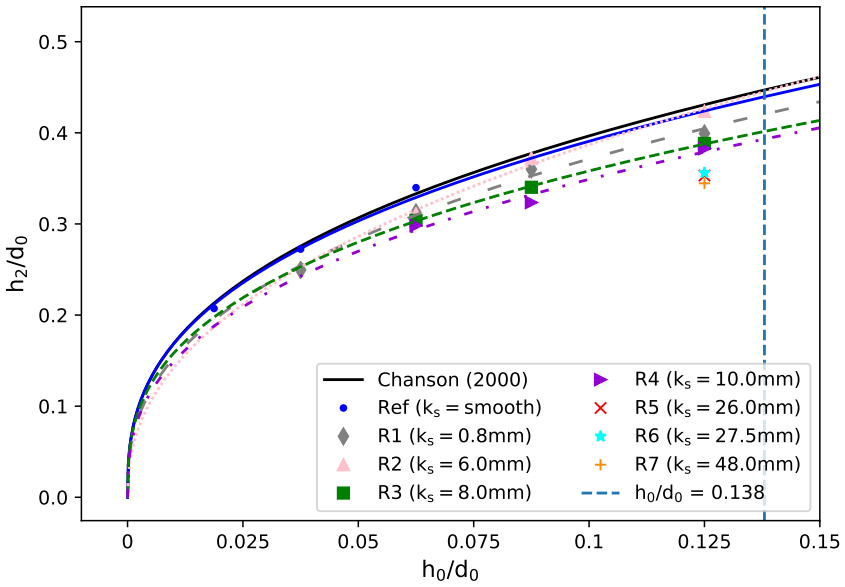

Figure E.2: Comparison of experimental obtained h_2 (k_s= 0.01, 0.8, 6.0, 8.0 and 10 mm tests with d_0= 0.4 m) and calculated h_2 values with Equation E.2 for increasing initially still water level in a range from dry bed to the limit h_0/d_0 = 0.138 imposed by Stoker (1957)

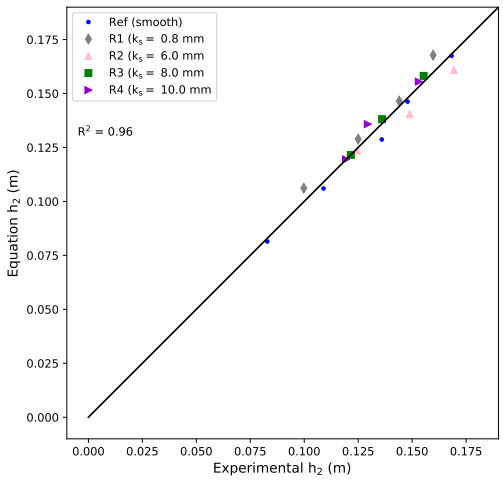

Figure E.3: Comparison of experimental obtained h_2 and calculated h_2 values with Equation E.2

The outcome of Equation E.2 (h_2 values) for several initially still water levels for tests with d_0 = 0.4 m can be seen in Figure E.2. Figure E.3 shows a comparison between the experimental obtained h_2 and the h_2 that is calculated with Equation E.2. The coefficient of determination (R^2) between all experimental plateau heights and calculated plateau heights is 0.96.

The presented empirical formula is not stated in the main report because the constants in the formula depend on the exact bed roughness values which must be researched more via a deeper analysis of the boundary. The approach used here to come up with the adapted formulas can be used when more accurate roughness values are obtained.